3 Lacustrine Sedimentology, Stratigraphy and Stable Isotope Geochemistry of the Tipton Member of the Green River Formation

Jennifer Walker Graf, Alan R. Carroll, and Michael Elliot Smith

Abstract

The Tipton Member of the Green River Formation occupies much of the Greater Green River Basin (GGRB) of Wyoming and Colorado. Long hypothesized to record a single shift from open to partly closed hydrology, new detailed stratigraphy and stable isotope geochemistry indicates that its strata record open, then partly closed, then open, then partly closed hydrology, which are each recorded by distinct transitions in facies associations, geochemistry, carbonate mineralogy, and organic content. Intervals of open hydrology occur coincident with the progradation of deltaic sandstones that are absent during the partly closed intervals, suggesting that environmental transitions were controlled by avulsions of the Idaho River. The first of these transitions occurs at the contact between the Scheggs bed and overlying Rife bed, and is thought to reflect the initial impoundment of Lake Gosiute. The Scheggs bed ranges from 23.5 to 36.5 m, and is characterized by fluvial-lacustrine lithofacies, calcitic mineralogy, an average Fischer Assay content of 7.6 gal./ton, and low $\delta^{18}O$ and $\delta^{13}C$ values (25.3‰ and 0.7‰, respectively). These deposits transition over a five meter interval to the overlying 2–15 m-thick lower Rife bed. The lower Rife bed is characterized by fluctuating profundal lithofacies, dolomitic mineralogy, an average Fischer Assay content of 17.6 gal./ton, and high $\delta^{18}O$ and $\delta^{13}C$ values (29.3 and 5.3‰). The lower Rife bed transitions up-section over a two meter interval into fluvial-lacustrine lithofacies

J.W. Graf (✉)
Encana Corporation,
370 17th St, Suite 1700, Denver, CO 80202, USA
e-mail: Jennifer.Graf@encana.com

A.R. Carroll
Department of Geoscience, University of Wisconsin-Madison, 1215 W. Dayton St., Madison,
WI 53706, USA
e-mail: carroll@geology.wisc.edu

M.E. Smith
School of Earth Science and Environmental Sustainability, Northern Arizona University,
602 S. Humphreys, Flagstaff, AZ 86011, USA
e-mail: michael.e.smith@nau.edu

M.E. Smith, A.R. Carroll (eds.), *Stratigraphy and Paleolimnology of the Green River Formation, Western USA*, Syntheses in Limnogeology 1, DOI 10.1007/978-94-017-9906-5_3

of the 2.5–20 m thick middle Rife bed, which exhibits calcitic mineralogy, an average Fischer Assay content of 9.7 gal./ton, and low $\delta^{18}O$ and $\delta^{13}C$ values (23.0 and 1.9‰). The third and final transition, from the middle Rife bed to the upper Rife bed, occurs gradationally over 6 m of section. The 6.5–22 m-thick upper Rife bed is characterized by fluctuating profundal deposits, dolomitic mineralogy, an average Fischer Assay content of 19.2 gal./ton, and high $\delta^{18}O$ and $\delta^{13}C$ values (29.8‰ and 8.5‰, respectfully). We interpret this succession of abrupt changes in lithofacies and isotope geochemistry within the Tipton Member to reflect the diversion, recapture, and ultimate diversion of a major source(s) of water and sediment into the basin.

3.1 Introduction

The Green River Formation (GRF) in the Greater Green River Basin (GGRB) records the dynamic evolution of Eocene Lake Gosiute as it transitioned from originally open paleohydrology to closed and then finally back to open paleohydrology before its final infilling by alluvium (Fig. 3.1) (Carroll and Bohacs 1999; Smith et al. 2008). The Tipton Member, previously the Tipton Shale Member (Schultz 1920), contains a broad array of non-marine facies. It underlies the evaporative Wilkins Peak Member, and has been proposed to record a transition from a hydrologically open to hydrologically closed lake basin (Roehler 1993; Pietras et al. 2003). Despite a long history of field and core-based investigation and documentation (Pipiringos 1955; Schultz 1920; Roehler 1992; Oriel 1961), the detailed stratigraphy and depositional controls of Tipton Member remain incompletely understood. This study represents a basin-scale examination of the lithofacies, stratigraphic packaging, and stable isotope geochemistry of the Tipton Member along White Mountain in the eastern Bridger subbasin of the GGRB. We argue that the Tipton Member records two compositionally and isotopically distinct transitions from overfilled to balanced-fill conditions.

The Tipton Member was deposited within the GGRB, which is located in the foreland of the Sevier fold and thrust belt, and is bounded by Precambrian-cored, Laramide-style uplifts to the north, south and east (Fig. 3.1) (Dickinson et al. 1988; DeCelles 1994). Basement-involved arches divide the GGRB into the Washakie, Sand Wash, Great Divide, and Green River sub-basins, all of which contain Tipton Member strata. Fluvial deposits of the Luman Member of the GRF and Niland Tongue of the Wasatch Formation underlie the Scheggs bed, whereas evaporative facies of the Wilkins Peak Member overly the Rife bed (Fig. 3.2). The Tipton Member has been divided into two beds: the Scheggs bed and overlying Rife bed (Roehler 1991b), the contact between which is understood to reflect a transition from freshwater, overfilled conditions to more saline, balanced-filled conditions within the lacustrine system (Roehler 1993; Carroll and Bohacs 1999). The Farson Sandstone, an arkosic deltaic complex, laterally bounds and interfingers with the Tipton Member in the northern part of the basin (Roehler 1992), and is equivalent to coarse-grained alluvial strata of the Pass Peak Formation in the northwest GGRB (Smith et al. 2008; Steidtmann 1969). Principal Tipton Member lithologies include variably organic-rich calcareous mudstone and marlstone, fossil-bearing siltstone, ostracode and oolitic grainstone, stromatolite, and various sandstone lithofacies assigned to the Farson Sandstone. Its fossil assemblages include freshwater bivalves and gastropods, fish, plant fragments, and vertebrate and invertebrate trace fossils. The Tipton Member is Early Eocene in age, based on late Wasatchian faunas found within it and in equivalent strata, and sanidine $^{40}Ar/^{39}Ar$ ages for ash beds contained within it and the overlying Wilkins Peak Member (Smith et al. 2008). Assuming that the

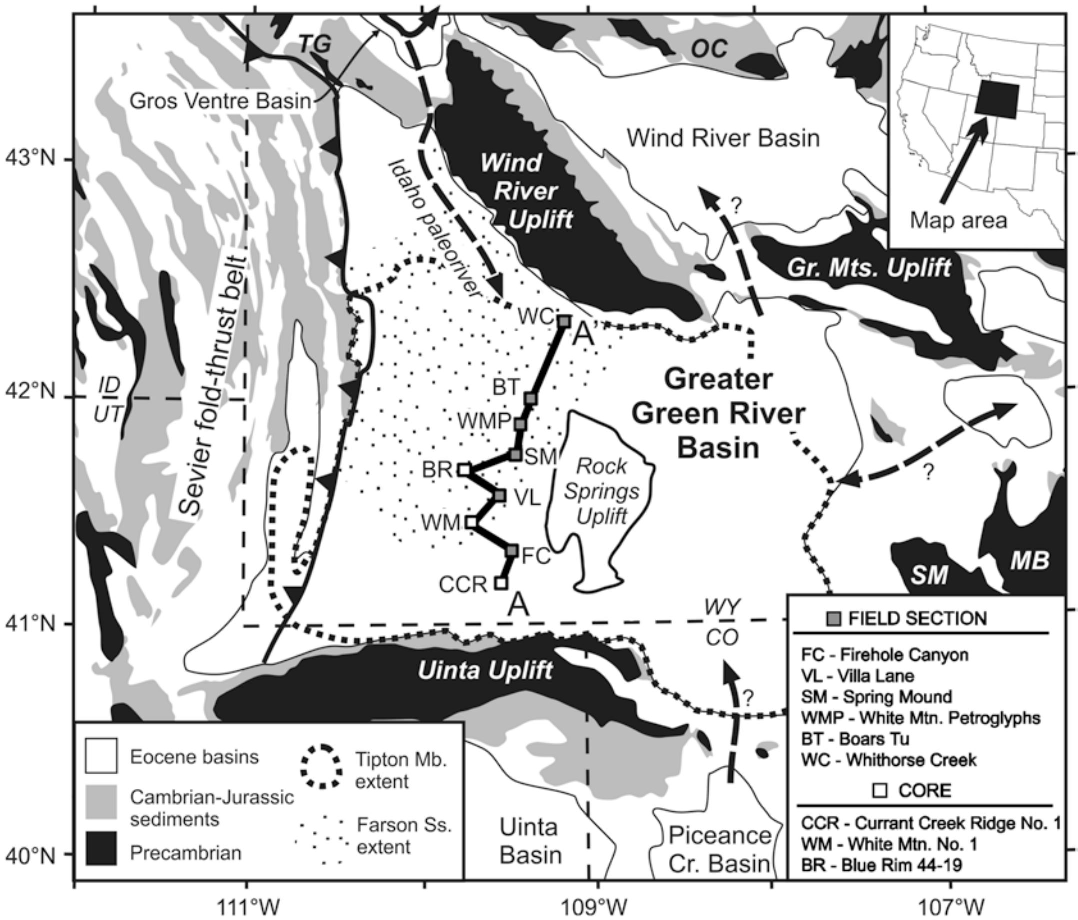

Fig. 3.1 Map showing the location of Eocene basins, basin-bounding uplifts, and measured sections (Base map modified from Witkind and Grose (1972). Abbreviations for Laramide uplifts: *TG* Teton-Gros Ventre, *OC* Owl Creek, *MB* Medicine Bow, *SM* Medicine Bow)

Scheggs bed represents 2/3 of the amount of time of the Lysitean mammalian subage, its deposition occurred over approximately 1.06 ± 0.43 m.y., (Smith et al. 2008, 2010). Based solely on their relative thicknesses, the Rife bed represents 0.60 ± 0.31 m.y. of deposition, whereas the Scheggs bed represents 0.46 ± 0.30 m.y.

3.2 Methods

3.2.1 Stratigraphic Analysis

Stratigraphic sections were chosen along a 150 km north–south cross-section through the GRB to document Lake Gosiute's evolution during deposition of the Tipton Member (Fig. 3.1). Five field sections were measured at decimeter-scale along the western and southwestern flanks of the Rock Springs Uplift along White Mountain and Flaming Gorge Reservoir. From the south to the north, they are Firehole Canyon (FC), Villa Lane (VL), Spring Mound (SM), White Mountain Petroglyphs (WMP), and Boar's Tusk (BT). An additional field section, Whitehorse Creek (WC), was modified from Pietras (2003) and incorporated into this study. Three cores supplement field data: the U.S. DOE/LETC Currant Creek Ridge No. 1 (CCR), U.S. ERDA White Mountain No. 1 (WM) and the Union Pacific Railroad Blue Rim 44-19 (BR). Locations of core and field sections are shown in Fig. 3.1.

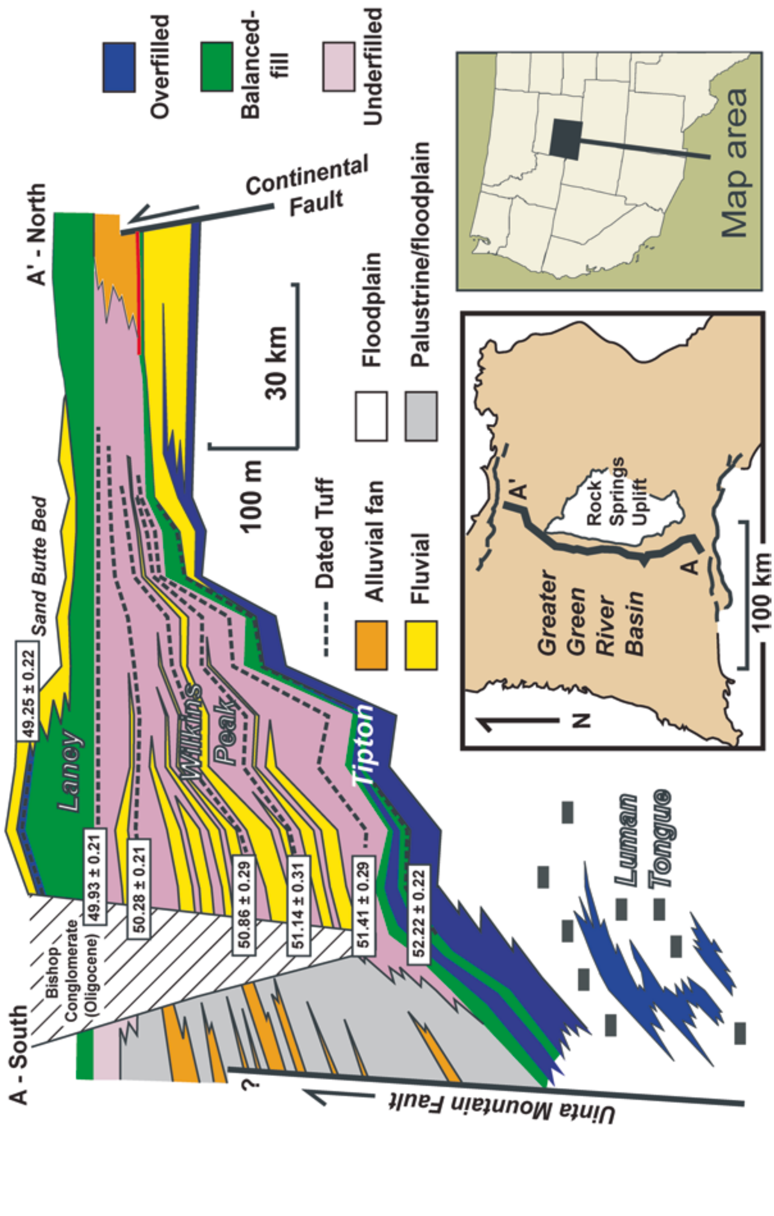

Fig. 3.2 Stratigraphy and associated lake-types of the Green River Formation in the Greater Green River Basin, Wyoming

3.2.2 Sampling

Field samples were collected primarily for comparative petrophysical analysis, and were not used for XRD and stable isotopic analysis due to observable effects of weathering. Samples from two cores, CCR and WM, were collected for XRD and stable isotopic analysis. The sample spacing and sample density of each core was concentrated on the Scheggs-Rife contact, as determined by lithofacies assemblages.

3.2.3 Mineralogy

The carbonate mineralogy of profundal mudstone samples from two cores (CCR and WM) was assessed using XRD analysis. Each sample was ground into fine powder, and a split of which was analyzed at the University of Wisconsin-Madison using a Sintag PAD V X-ray diffractometer using a Cu Kα x-ray source (λ = 1.5418 Å). The scans of 54 samples were run between 20 and 55 degrees 2-θ, a range that captures all relevant calcite and dolomite peaks. Step size was set at 0.02 degrees, with a step time of 1 s. The calcite-dolomite proportion of each sample was determined using the relative areas of dominant calcite peaks (those between 29.30 and 30.00 degrees 2-θ) and dolomite peaks (those between 30.40 and 31.10 degrees 2-θ) according to the relationship:

$$\%_{calcite} = \left[\frac{\sum A_{calcite\_peak}}{\left(\sum A_{calcite\_peak} + \sum A_{dolomite\_peak} \right)} \right] * 100$$

Based on this calculation, samples were categorized as dominantly calcitic (>80 % calcite), mixed (20–80 % calcite), or dominantly dolomitic (<20 % calcite).

3.2.4 Stable Isotopes

An additional split of each powdered sample was allocated for geochemical analysis. Samples were processed at the University of Michigan Stable Isotope Laboratory in Ann Arbor, Michigan where they were roasted in vacuo at 200 °C for 1 h to remove contaminants. Samples were then reacted at 77° ± 1 °C with 4 drops of anhydrous phosphoric acid for 8 min (12 min for dolomitic samples) in a Finnigan MAT Kiel IV preparation device coupled directly to the inlet of a Finnigan MAT 253 triple collector isotope ratio mass spectrometer. Maintained measured precision using this methodology is reported as better than 0.1 ‰ for both carbon and oxygen isotope compositions. In this study, $\delta^{18}O$ data is reported relative to VSMOW, while $\delta^{13}C$ data is reported relative to VPDB. Where duplicate samples were run, averages weighted according to standard deviation were used.

3.3 Lithofacies

This study recognizes 13 lithofacies within the Tipton Member, as defined by lithology, organic content, sedimentary structures, biologic markers and paleo-flow indicators (Table 3.1).

Microlaminated kerogen-rich mudstone Laminated, organic-rich mudstone is the dominant lithofacies of the Rife bed, though it is also found to a lesser extent in the Scheggs bed. The mudstone is generally dark-brown to black in color. Discrete, rhythmic, variegated laminations are μm to mm in scale, and planar parallel (Fig. 3.4a). Interlaminations (mm- to cm-scale) of tan siltstone, tuff, and chert are found infrequently within sections. Fischer Assay oil yields range between 20 and 28 gal./ton (Roehler 1991a), qualifying these rocks as high-quality oil shale (Culbertson et al. 1980; Dana and Smith 1972). Well-preserved, intact fish fossils are present though infrequent. Occasional phosphatic concretions are preserved as both thin (mm-scale), lenticular bodies along lamination planes as well as irregularly shaped nodules around which overlying laminations are deformed. When associated with thin interbeds of sand, stromatolite, and ostracode and oolitic grainstone, cm-scale mud cracks are observed. In outcrop, this lithofacies forms pronounced cliffs that can be

Table 3.1 Tipton Member Lithofacies

Lithofacies	Description	Occurrence	Interpretation
Microlaminated kerogen-rich mudstone	Dark brown to black mudstone with µm- to mm-scale laminations, high kerogen content, no intact biologic markers; Fischer Assay yield of 20–28 Gal./ton	Primarily found in Zones B and D. It is present in meter-scale intervals throughout CCR and in the upper- most portion of WM's Zone C	Profundal deposition in anoxic water bottoms devoid of bioturbating benthic organisms
Laminated mudstone	Grey to brown mudstone with densely spaced, varigated, µm- to cm-scale laminations, including interlaminations of silt and tuff. Fish, ostracodes, burrows and coprolites are present; Fischer Assay yield of 9–22 Gal./ton	Observed in all zones of all sections, excluding WC	Profundal deposition in anoxic water bottoms devoid of bioturbating benthic organisms
Massive kerogen-rich mudstone	Dark brown to black mudstone with no visible laminations, high kerogen content, intermittent silt and kerogen-stained tuff interlaminations; Fischer Assay yield of 22–26 Gal./ton	Minor component of Zones B and D, though is infrequently observed throughout all Zones in CCR	Profundal deposition in anoxic water devoid of bioturbating benthic organisms
Massive mudstone	Grey mudstone with no visible laminations. Abundant gastropods and bivalves and infrequent burrows are present; Fischer Assay yield of 2–6 Gal./ton	Primary component of the basin- ward associations of Zones A and C	Littoral to sub-littoral deposition via hyperpycnal plumes during storms and/or bioturbation of originally laminated mud
Fossiliferous siltstone	Grey or tan siltstone with gastropods and bivales (Scheggs) and fish (Rife) fossils. Laminations are low, density, mm- cm-scale with varied orientations	Found throughout all zones in CCR, BR, BT, WC. Primarily Zones A and B in WM, Zone C in VL, A and D in SM, and Zones A, C, and D in WMP	Littoral margi, pro-delta/distal bar, or turbidite, depending on lithostratigraphic context
Delta foreset sandstone	Steeply-dipping (29 degrees) foresets of vF-F, subangular, well-cemented sand bearing cm-scale rip-ups of underlying silt	Observation is exclusive to the Farson Sandstone in Zone A at WMP	Deposition by grain flow avalanches down the front of a Gilbert-type delta
Trough cross-bedded sandstone	Vertically aggregated bed sets of vF to M sized, angular to subangular sand. Laminae dip 25 degrees and are distinguished by mica- rich laminae	Most prevalent sandstone architecture; Found in Zone A and C sands	Delta channel mouth bar deposition by ripples and dunes formed under unidirectional flow
Horizontally-bedded sandstone	Vertically aggregated, horizontal beds of vF sand that display slight fining upwards trend. Burrows, reed imprints are present	Frequent component of Zone A and C sands at WM, VL, SM, WMP, BT, and WC	Upper shoreface deposition at distributary terminii by unidirectional flow and/or swash zone deposition along beach faces

(continued)

Table 3.1 (continued)

Lithofacies	Description	Occurrence	Interpretation
Hummocky cross-stratified sandstone	Hummocked bed sets with 1–3 mm laminations dipping 15 degrees. Micaceous laminations and entrained fish debris are present	Observed in BR core and in Zone C at WMP field station	Storm-dominated lower shoreface
Climbing-rippled to wavy-bedded sandstone	Vertically aggregated, variably sinuous laminations of vF sand	Observed in Zone A of WMP and BT; Zone C in WMP	Delta-front deposition during period of high sedimentation
Massive sandstone	Grain-supported, vF-M sand lacking internal architecture. Rip-ups, burrows, floral material and fish debris are often present	More frequent Zone A sands (BR, VL, WMP, BT, and WC), but also observed in Zone C (BR and BT)	Liquefied delta slump/ debris flow deposition or intensely bioturbated delta front or lower shoreface deposit
Stromatolite	Brecciated isolated carbonate mounds (Scheggs) and laterally extensive stromatolites associated with green, mud-cracked, mineral-bearing siltstone (Rife)	Brecciated stromatolite exclusive to Zone A at SM. Laterally extensive stromatolites observed in Zone A of SM and Zone D in FC, SM, WMP and BT	Isolated tufa-travertive subaqueous spring deposits in the Scheggs bed; Widespread littoral stromatolitic carbonate deposition mediated by microbial mats in the Rife bed
Ostracode and ooid grainstone	Medium to coarse grain-sized, preserved as horizontal laminations and within vertical burrows, and often entrain silt rip-ups, fish debris and phosphatic resins	Found in the Rife Bed at CCR, BR, SM, WMP, and BT. Within the Scheggs bed, it is found only in CCR core. Observed in Zone A (CCR, SM), Zone B (CCR, BT), Zone C (BR), and Zone D (BR, SM, WMP)	Deposition of carbonate allochems in shallow, wave-agitated lake margin areas where Ca-rich stream/ spring waters and lake waters interacted

Notes: Abbreviations indicating modal grain size of sandstone: *M* medium, *F* fine, *vF* very fine.

traced laterally for tens of kilometers. Field sections weather blue in color, and are colloquially referred to as "blue beds".

Interpretation: Preservation of fine, densely spaced laminations suggests deposition from suspension in an area beneath wave base and where bottom currents were continuously slow or non-existent. The high rate of organic preservation, reflected by high Fischer Assay oil yields, is interpreted to reflect deposition within low-oxygenated or entirely anoxic water conditions (e.g. Demaison and Moore 1980). However, it is unresolved whether permanent chemical and thermal stratification of lake waters is necessary for generation of kerogen-rich laminated mudstone (i.e., oil shale). Citing the presence of fossil catfish within oil shale lithofacies of the Laney Member of the GRF, Buchheim and Surdam (1977) suggested that only fluctuating or semi-permanent lake stratification is necessary for oil shale deposition within the GRF. An alternative interpretation of the presence of bottom-dwelling catfish within oil shale, however, is that the corpse bloated, floated out to deeper areas of the lake where it sunk and then came to rest along anoxic bottom waters.

The small phosphatic nodules around which overlying laminae conform are interpreted as coprolites, an observation also reported in profundal sediments of the Tipton Member (Castro 1962) and the Laney Member (Fischer and Roberts 1991). This facies is interpreted to represent profundal lacustrine deposition within a low-oxygenated, stratified lake conditions similar to those found within profundal zones of modern lakes Zurich (Bradley 1929; Kelts and Hsü 1978) and Tanganyika (Huc et al. 1990).

Laminated mudstone This lithofacies is represented in both the Scheggs and Rife beds as grey to brown mudstone. In most examples, variegated laminations range between mm to cm in scale (Fig. 3.3b). Upper and lower contacts of distinct laminae are variable, occurring as discrete planar, diffuse/gradational planar, or wavy/irregular. Infrequent mm- to cm-scale interlaminations of grey-tan silt and tuff are also present. Within the mudstone and siltstone inter-laminations, well-preserved fish fossils, ostracode molds, and compacted, vertical burrows are present. Tan, spherical nodules of silt onto which overlying laminae conform are observed with variable frequency. Fischer Assay oil yields range between 9 and 22 gal./ton (Roehler 1991a), classifying this lithofacies as low-quality oil shale (Culbertson et al. 1980; Dana and Smith 1972). Outcrop expression ranges from covered, gradual slopes to moderately high-angle cliffs.

Interpretation: The relatively diminished Fischer Assay oil yield of this lithofacies compared to that of the mm-laminated, organic-rich mudstone lithofacies suggests either diminished organic production, an increase in organic destruction and/or clastic dilution. The primary source of oil-shale kerogen in the GRF is autochthonous algae and bacteria (Tissot and Vandenbroucke 1983; Horsfield et al. 1994; Carroll and Bohacs 2001; Bohacs et al. 2000). During periods of sustained freshwater input, a corresponding increase in available oxygen may have increased degradation of these particulate organics (Horsfield et al. 1994), while increased inorganic sedimentation may have diluted preserved organic concentrations (cf. Carroll 1998). Alternatively, freshwater input has been attributed to the reduction of dissolved bicarbonate concentrations within a lake system, which ultimately decreases primary productivity (Horsfield et al. 1994). Collectively accounting for each possibility, this lithofacies is interpreted to reflect deposition during periods of freshwater input and low chemical and thermal stratification.

Massive kerogen-rich mudstone Massive, organic-rich mudstone is present in the Rife bed and, less frequently, in the Scheggs bed. This mudstone is typically dark-brown to dark grey in color. Laminations are not visible in hand samples or thin section, but may exist cryptically. Silty interbeds are rare, and thin (mm-scale) interlaminations of bitumen-saturated tuff and horizontal fracture-fills of dolomite are frequently observed. Fischer Assay yields range between 22 and 26 gal./ton (Roehler 1991a), qualifying this mudstone as high-quality oil shale (Culbertson et al. 1980; Dana and Smith 1972). Both core and field samples have a bituminous odor and are absent of well-preserved burrows, ostracode molds and fish fossils. Outcrop expression of this facies is pronounced cliffs that can be traced laterally for several kilometers.

Interpretation: Like the laminated organic-rich mudstone, above, preserved organic matter suggests sub-mixolimnium deposition in a chemically and thermally stratified lacustrine system in which there was an insufficient alternation in the delivery of micrite to create lamination. Massive kerogen-rich mudstone beds could also have been deposited by hypopycnal plumes basinward of sites of fluvial input or created via entrainment of organic rich mud during storm events (cf. Renaut and Gierlowski-Kordesch 2010).

Massive mudstone Massive mudstone is the dominant lithofacies of the Scheggs bed. It is almost exclusively light to medium grey in color, has no visible lamination, and generally preserves largely intact freshwater animals such as gastropods (2–4 cm) and bivalves (4–8 cm) (Fig. 3.3c and d), both of which commonly exhibit abrasion and removal of shell ornamentation. Ostracodes are abundant throughout, whereas vertical burrows occur infrequently. In the lower Scheggs bed, gastropods and bivalves are commonly silicified. Towards the upper Scheggs bed, however, gastropods become less frequent and articulated bivalves retain original aragonite mineralogy. The Fischer Assay oil

Fig. 3.3 Photographs of Tipton Member lithofacies: (**a**) Thinly laminated (μm to mm), organic-rich mudstone; (**b**) variably laminated (μm to cm) mudstone; (**c**) silicified *Goniobasis tenera* gastropods, which constitute the *Goniobasis* Marker bed; (**d**) freshwater bivalves preserved in the fossil-bearing siltstone lithofacies; (**e**) Gilbert-type foresets observed from the WMP section; (**f**) climbing ripples resulting from super-critical flow with both stoss- and lee-sides preserved; (**g**) injection feature where vF sand is injected into overlying F sand in the BR core; (**h**) concentric delamination of stromatolites which mark the Tipton-Wilkins Peak contact; and (**i**) brecciated stromatolites at the SM field section

yield of this lithofacies is low, ranging between 2 and 6 gal./ton (Roehler 1991a). Deep trenching (~0.5 m) did not reach un-weathered, intact section due to vegetated slopes. Abundant silicified float is, therefore, the primary facies identifier in the field. It should be noted that the observation of aragonitic fossils in the field was limited to the Villa Lane section, where a recent road cut had generated fresh exposure.

Interpretation: The absence of lamination within this lithofacies suggests either continuous sedimentation (Pasierbiewicz and Kotlarczyk 1997), or more likely the bioturbation of formerly laminated mud (Fischer and Roberts 1991; Demaison and Moore 1980) within a non-stratified lacustrine system (Bradley 1929, 1931; Carroll 1998). It may also reflect deposition by hyperpycnal plumes delivered to the lake center during periods of significant fluvial input or shoreface agitation by waves. The decreased kerogen content observed within this lithofacies is thought to reflect algal degradation resulting from increased oxygenation and decreased bicarbonate due to downstream outflow of lakewaters (Horsfield et al. 1994). This study interprets the massive mudstone lithofacies as littoral deposits within a freshwater system, which is consistent with the observation by Surdam and Stanley (1979) of bioturbated, mollusk and ostracode-bearing mudstone with freshwater deposits of the upper Laney Member of the GRF, as well as the observation of Cohen (1989) of abundant gastropod infauna within the littoral to sub-littoral zones of modern Lake Tanganyika.

Fossiliferous siltstone Fossil-bearing siltstone is found in both profundal and marginal deposits. It is medium grey or tan in color and is either laminated or massive. Laminated intervals display mm- to cm-scale laminations of varied shades of brown silt and mudstone. Contacts among laminations occur as planar-parallel, wavy-parallel, and wavy non-parallel. Mollusc and ostracode fossils are most commonly associated with planar-parallel and massive interbeds. Where thicker than approximately 0.5 m in outcrop, this lithofacies typically constitutes low-angle, vegetated slopes that require trenching (<0.25 m) for stratigraphic observation. Exposure quality of thin interbeds of this lithofacies (<0.5 m) is highly variable and largely dependent upon the resistance of overlying lithologies.

Interpretation: This lithofacies is found within a variety of depositional and hydrodynamic environments. Where siltstone contains abundant gastropods that are continuously distributed throughout the bed, this lithofacies is interpreted to represent littoral deposition. Similarly dense gastropod concentrations are observed in the littoral margins of Lake Tanganika (Cohen 1989). Where this lithofacies occurs as thin, fining-upward interbeds within mudstone lithofacies, it is interpreted as turbidite deposits. In association with stacked, coarsening upward successions of sandstone and mudstone, the siltstone lithofacies is interpreted as pro-delta and distal bar deposits. Similar pro-delta deposits are observed in the Laney Member of the GRF (Stanley and Surdam 1978), in Late Pleistocene Lake Bonneville (Lemons and Chan 1999), and in Jurassic deposits within the East Gobi Basin, Mongolia (Johnson and Graham 2004).

Delta foreset sandstone Within this study area, steeply dipping delta foreset lithofacies are limited to the Farson Sandstone Member at the WMP and WC (Pietras 2003) field sections. At WMP this lithofacies constitutes approximately 4.5 m of vertical section. Foresets dip 28 degrees (Fig. 3.3e) and are composed of micaceous, biotite-rich, vF-F, sub-angular sandstone that is well-cemented by calcite. Relatively large (up to 4 cm) rip-ups of underlying tan siltstone are observed along foreset planes, while twig and reed impressions are found less frequently. Irregular, 10–20 cm loading features typify the contact of this facies with underlying, convoluted siltstone. The upper portion of the steeply dipping foreset lithofacies is typically abruptly overlain by mudstone.

Interpretation: The steeply dipping foresets of this lithofacies are interpreted as delta front deposits. A high flow regime, capable of transporting terrigenous plant material basin-ward and eroding cohesive mud and siltstone, is thought to have existed during deposition. Soft-sediment deformation within underlying units suggests this lithofacies was deposited rapidly across a soft substrate, while bed thickness indicates water depth was at least 4.5 m. Accounting for compaction effects, foreset height and interpreted water depth may have been greater. Larger (25 m) Gilbert-type foreset beds are observed in Eocene Fossil Lake (Buchheim and Eugster 1998) and within Upper Laney Member of the Green River Formation (Stanley and Surdam 1978). Modern analogues include deltaic deposits in freshwater lakes Constance (Müller 1966), Pyramid (Born 1972) and Malawi (Scholz et al. 1993).

Trough cross-bedded sandstone This lithofacies is a dominant component of the Farson Sandstone and is observed in both field and core sections. Beds are 10 cm–4 m thick and are composed of vertically aggraded sets that range between 5 cm and 25 cm in thickness and approximately 15–40 cm in width. Individual mm- to cm-scale bedding planes consist of grain-supported, angular to sub-angular, vF to M sand. Bounding surfaces between sets curve approximately 25 degrees at their steepest, and are tangential to underlying erosion surfaces. Laminae are often highlighted by concentrations of biotite and muscovite. No visibly identifiable floral or faunal remnants are preserved. Outcrop relief of this lithofacies is highly variable and dependent upon localized weathering effects.

Interpretation: Trough cross-beds occur in a variety of depositional environments, where flow is sufficient for the down-flow migration of dune structures (Allen 1962; Harms and Fahnestock 1965). In association with stacked sequences of laminated mudstone, siltstone and sandstone, this lithofacies is interpreted to represent delta slope and channel deposits. Similar trough cross-bedded deposits are documented in the Bitter Creek deltaic complex of the Laney Member (Stanley and Surdam 1978), as well in Jurassic-Cretaceous lacustrine deltas in the East Gobi Basin, Mongolia (Johnson and Graham 2004).

Horizontally-bedded sandstone Horizontally bedded sand is exclusive to the Farson Sandstone and is observed in both core and field sections. Packages are between 20 cm and 2 m thick, and are composed of 2–5 mm thick, horizontal to near horizontal (less than 2 degree dip), vertically aggregated beds of vF sand, which are distinguished by muscovite- and biotite-rich interlaminations. Infrequently, vertical burrow structures, reed and twig imprints, and cm-scale interbedded tuffs are observed.

Interpretation: Horizontally laminated sandstone within the Farson Sandstone suggests deposition within high flow regimes (Harms and Fahnestock 1965; Bridge 1978; Paola et al. 1989; Arnott and Southard 1990; Cheel 1990; Arnott 1993). Typically found at the top of coarsening-upward packages of littoral mudstone, siltstone and sandstone, we study interprets horizontal laminations to have been deposited by shallow, high energy unidirectional flow and/or bidirectional wave-generated currents in a swash zone along upper delta-front and delta margins.

Hummocky cross-stratified sandstone Micro-hummocky cross-bedded, vF sand is limited to Farson Sandstone deposits and is observed in both core (BR) and field (WMP) sections. Individual laminations are approximately 1–3 mm and dip approximately 15 degrees. Distinguished by mica-rich laminations, bed sets range between 3 and 6 cm thick, while aggregated packages of bed sets range between 10 and 25 cm in thickness. In the WMP field section, hummocks entrain abundant phosphatic fish "debris" composed of broken ribs, scales, platelets and vertebrae. Outcrop exposure of this lithofacies is highly variable and largely dependent upon the resistance of overlying lithofacies.

Interpretation: Hummocks result from a combination of oscillatory and weak unidirectional flow (Nøttvedt and Kreisa 1987; Leckie and Krystinik 1989; Arnott and Southard 1990; Dumas et al. 2005) in an environment where sedimentation rates are high and water depth low enough to facilitate large, fast waves, yet deep enough to maintain the oscillatory waves and unidirectional currents (Dumas and Arnott 2006). In association with stacked successions of mudstone, siltstone and sandstone lithofacies, hummocks are interpreted to have formed in the littoral zone under combined-flow between fairweather and storm wave base, likely in upper delta-front and lower delta-platform environments.

Climbing-rippled sandstone This lithofacies is exclusive to the Farson Sandstone and is observed in both core and field section. Beds are between 0.3 and 1.5 m thick, and are composed of 2 mm to 4 cm thick vertically aggraded, variably undulating laminations of vF sand that are made distinct by intermittent silt-, muscovite- and biotite-rich laminations (Fig. 3.3f). Ripple limbs exhibit irregular sinuosity, dipping between 15 and 30 degrees on either side of the ripple crest. Unlike the planar parallel and hummocky sand lithofacies with which this lithofacies is commonly associated, organic matter and fossils are not observed. Outcrop expression is highly variable and largely dependent upon the resistance of overlying lithofacies.

Interpretation: Preservation of both the lee and stoss limbs of each ripple crest indicate deposition in an area having high rates of sedimentation from suspension and bed load (Jopling and Walker 1968; Allen 1982). Variability of inclination among the ripple limbs of this lithofacies is thought to be a function of small changes in the hydrodynamic environment and/or variable sediment discharge. As part of the Farson Sandstone, this lithofacies is interpreted to represent deposition along the delta-front, an area known for high-rates of sedimentation and wave-action modification thereof (McLane 1995).

Massive sandstone The massive sandstone lithofacies is exclusive to the Farson Sandstone, and is observed in both core and field sections observed as beds of vF to mL, grain-supported sandstone that occur in 10 cm–4 m intervals. Silt and mud rip-ups, fish debris, burrows preserved by differential cementation, and terrestrial plant material such as reeds and root casts are commonly observed throughout the beds. Internal architecture, however, is absent. Underlying siltstone frequently exhibits scour and convolute bedding due to loading of overlying sandstone. Grain-size within the sandstone beds is variable, ranging from vF to mL. Transitions between sandstone grain-size are often, but not always, abrupt. Where contacts are sharp, load-induced injection, or flame structures, are observed (Fig. 3.3g).

Interpretation: Lack of internal architecture within this lithofacies is interpreted to result from either liquefaction related to delta slump processes or bioturbation along the delta-top or delta shore-face. Where underlying sediments exhibit deformation, slumping is thought to have occurred, while burrows, though limitedly preserved, indicate bioturbation along shore-face or delta top environments. Stanley and Surdam (1978) observed similar massive units along the shore-face of the Bitter Creek deltaic complex in the Laney Member.

Stromatolite Though algal stromatolites are present in both the Rife and Scheggs beds, distinct morphological properties and depositional environments differentiate the two occurrences. Stromatolite beds within the Rife bed are 10–30 cm thick, weather orange-brown by concentric spalling (Fig. 3.3h), and are laterally extensive across several kilometers. Here, stromatolite beds are associated with a transition from organic-rich calcareous mudstone to green, mud-cracked, evaporite mineral-bearing siltstone. As such, this facies is interpreted as the base of the Tipton-Wilkins Peak contact. The stromatolite lithofacies in the Scheggs bed is exclusive to the Spring Mound (SM) field section and is laterally bound approximately 20 m to the north and south by two large (12 m high × 20 m wide) spring deposits with which it inter-fingers. The stromatolite package itself constitutes 40 cm of vertical section. The upper 30 cm of this is a breccia consisting of pebble- to gravel-sized clasts of broken algal material, shale and silt rip-ups (Fig. 3.3i).

Interpretation: Modern lacustrine stromatolite beds are observed along many lake margins and adjacent fluvial systems, such as Green Lake (Eggleston and Dean 1976), the Great Salt Lake (Halley 1976), and Lake Tanganyika (Cohen and Thouin 1987; Cassanova and Hillaire-Marcel 1992). Within the Rife bed, stromatolite beds are inferred to have formed near the shore, similar to those found in the Laney Member (Wolfbauer and Surdam 1974; Roehler 1993; Rhodes 2002). However, in the absence of an observable shore-parallel transect within the GGRB, neither this study nor Laney Member studies can confirm whether stromatolite beds are linear, shore-parallel features. Previous studies have not reported stromatolite beds in the Scheggs bed. It is likely that the high rates of hydrologic influx, corresponding shoreline transgressions and the chemical parameters of an overfilled lacustrine system prevented extensive growth. The structural high and local calcium ion-rich geochemistry of the spring mounds are interpreted to have enabled stromatolite growth and preservation at the Spring Mound field section. From the morphology and preservation characteristics, we infer that stromatolite beds within the Scheggs bed were initially protected by adjacent mound structures, but increased wave action resulting from lake expansion re-worked and brecciated the algal mats.

Ostracode and ooid grainstone Ostracode and oolitic grainstone lithofacies are found in both the Scheggs and Rife beds. Medium to coarse grain-sized, undeformed ostracodes and oolites are preserved as horizontal laminations (2 mm–7 cm) and within vertical burrows. In both occurrences, ostracodes and oolites are associated with fossil-bearing siltstone, cm-laminated mudstone, and massive sandstone facies. Entrained within the grainstones are small (mm- to sub-mm) silt rip-ups and phosphatic fish debris, including scales, ribs, vertebrae and articulated jaws. The lithologic texture of the grainstone is generally friable in outcrop and loosely consolidated in core.

Interpretation: Though ostracodes are found throughout many lacustrine sub-environments (Cohen 2003), accumulation and formation of skeletal debris into a grainstone requires hydrologic sorting and/or minimal clastic dilution, suggestive of wave agitation along shorelines far from fluvial deltas. Oolites are similarly observed along wave-agitated lake margins (Cohen and Thouin 1987; Talbot and Allen 1996; Balch et al. 2005) where groundwater and lake water mixing leads to precipitation of inorganic carbonate (Wolfbauer and Surdam 1974; Kelts and Hsü 1978).

3.4 Lithofacies Assemblages and Associations

Two distinct lithofacies assemblages comprise the Tipton Member: fluvial-lacustrine and fluctuating profundal, both of which have distinct basin-ward and shoreward associations (Table 3.2; Fig. 3.4). Together, these lithofacies assemblages define four stratigraphic zones within the Tipton Member. The fluvial-lacustrine lithofacies assemblage defines the Scheggs bed (Zone A), while both fluctuating-profundal (Zones B and D) and fluvial-lacustrine assemblages (Zone C) characterize the overlying Rife bed (Fig. 3.2). These stratigraphic zones correspond to distinct zones of carbonate mineralogy as determined by XRD analysis. Profundal mudstone of fluvial-lacustrine Zones A and C is dominantly calcitic (69 % and 80 % calcite, respectively), while profundal mudstone of fluctuating-profundal Zones B and D is dominantly dolomitic (30 % and 12 % calcite, respectively).

3.4.1 Fluvial-Lacustrine Lithofacies Assemblage

Basin-ward association The dominant component of this association is the massive mudstone lithofacies, which bears abundant bivalves and gastropods (Fig. 3.5a). Interlaminations of fining upward beds (3–60 cm thick) of fossil-bearing siltstone lithofacies, which also preserve broken freshwater taxa, are frequent. Within the bottom-most cored meters of the CCR core, both massive and laminated organic-rich mudstone lithofacies contain interbeds of coquina. These interbeds range between 1 and 75 cm thick and contain bivalve and gastropod shell fragments within an organic-rich mudstone matrix. While the majority of these interbeds preserve primary aragonite, the largest interbed (75 cm) is has noticeably less mudstone matrix and is calcified throughout.

The basin-ward association of this assemblage reflects sustained water and sediment input into a hydrologically open, non-stratified lake system.

Table 3.2 Tipton Member Lithofacies Associations

Association	Dominant lithofacies	Occurrences	Interpretation
Fluvial lacustrine assemblage			
Basin-ward	Massive mudstone; fossiliferous siltstone (gastropods and bivalves); isolated occurrence of laminated mudstone containing bivalves.	Zone A (CCR, WM, VL, and upper portion in SM) and Zone C (CCR, WM).	Sustained high-stand conditions within a well-oxygenated, open lake system.
Shoreward	Coarsening-upward successions of massive sandstone; delta foreset sandstone; trough cross-bedded sandstone; horizontally-laminated sandstone; climbing-rippled sandstone; hummocky cross-stratified sandstone; gastropod coqina; fossil-bearing silstone (gastropods and bivalves).	Zone A (BR, SM, WMP, BT and WC) and Zone D (WM, VL, BR, SM, WMP, and BT).	Laterally migrating delta fan complex indicating sustained water and sediment influx into the lake.
Fluctuating profundal assemblage			
Basin-ward	Microlaminated kerogen-rich mudstone; massive kerogen-rich mudstone; fossil- bearing siltstone (fish); common tuff interlaminations.	Zone B (CCR, WM, VL, BR, SM, WM, and WMP) and Zone D (CCR, FC, WM, VL).	Continuous profundal deposition within a repeatedly oscillating closed, stratified lake system.
Shoreward	Thin beds of massive sandstone; fossiliferous siltstone; stromatolites, and ostracode and ooid grainstones.	Zone B (BT and WC) and Zone D (BR, SM, WMP, BT, and WC).	Littoral environments on the edge of a rapidly oscillating saline lake.

Abundantly preserved salt-sensitive fauna (e.g. bivalves) indicate well-oxygenated, freshwater conditions within the lake, while the absence of mudstone lamination and tuff interbeds suggest a combination of bioturbation, continuous sedimentation, and mixing within the suspended sediment column during deposition. Decreased Fischer Assay oil yield within fine-grained sediments is also evidence of sustained water and sediment input. Where fluvial systems enter a lacustrine basin, the concentration of particulate organics is reduced by clastic dilution, chemical degradation due to well oxygenated source waters, biologic consumption, or a combination thereof (Huc et al. 1990; Horsfield et al. 1994; Bohacs 1998). The effects of these processes are assumed to be greater in areas more proximal to source water input. The lateral expanse (>50 km of the study area) to which fine-grained profundal sediments of this association are depleted of kerogen is interpreted to reflect basinwide oxygenation and increased water and sediment input to the basin. Moreover, stacked 10–100 cm alternations between organic-rich and organic-depleted mudstone are not observed in this assemblage, which we interpret to reflect sustained hydrologic input and corresponding lake-level high-stand (Bohacs et al. 2000). Horsfield et al. (1994) observe similar lack of thin parasequences within fluvial-lacustrine deposits of the underlying Luman Tongue.

Organic-rich mudstone in Zone A of the CCR core is thought to reflect deeper, less-oxygenated waters beyond the effects of clastic dilution. At this location, Fischer Assay oil yield is greater (10.8 gal./ton) than that observed among fine-grained lithofacies located more proximal to the deltaic complex of the Farson Sandstone (e.g. 4.5 gal./ton at WM). Roehler (1992) for example interprets the CCR core location as one of the deepest areas of Lake Gosiute. Because the organic-rich mudstone lithofacies suggests anoxic or low-oxygenated bottom waters, interbeds of broken aerobic fauna are interpreted as

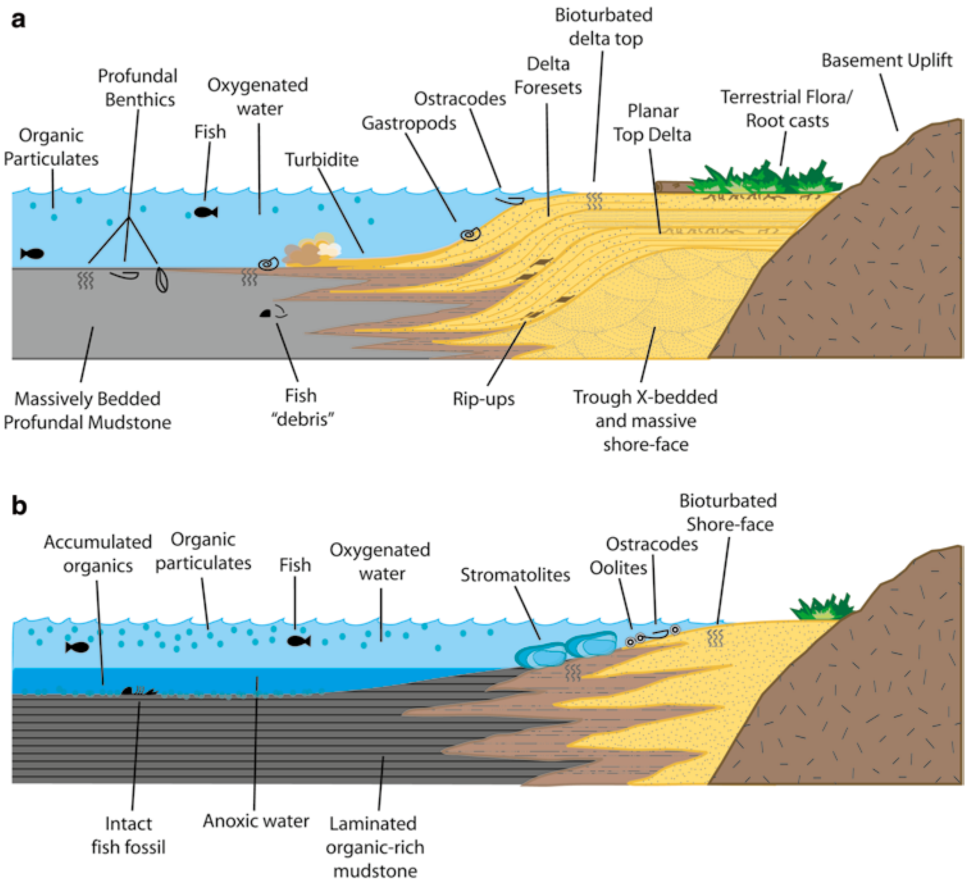

Fig. 3.4 Schematic interpretive cross-section of Lake Gosiute during (**a**) fluvial-lacustrine and (**b**) fluctuating profundal deposition

turbidite deposits. Gravity currents, similar to those described in Kneller and Buckee (2000), are thought to have transported these fauna basin-ward from shoreline and littoral habitats. In this manner, finer-grained sediment entrained in the current, such as silt and littoral mud, would have been deposited further basin-ward. Up-section within CCR core, small beds (5–15 cm) of fining-upward silt are interpreted as distal deposits of gravity currents.

Shoreward association Coarse-clastic deposits of the Farson Sandstone typify the shoreward association of the fluvial-lacustrine assemblage. Concentrated to the northern-most portion of the basin, stacked, coarsening-upwards successions of laminated mudstone, siltstone and sandstone lithofacies (Fig. 3.5b) are interpreted to represent a broad deltaic sequence, which grades basin-ward to laminated profundal mudstone. Mudstone lithofacies represent pro-delta deposits, siltstone lithofacies the distal bar, and sand lithofacies delta front and delta top deposits. Overall thickness of these successions decreases basin-ward, while the number of sequences and ratio of fine-grained sediments to sand increases. Load-induced contacts (e.g. Fig. 3.3g) are found between the gastropod-bearing siltstone and overlying trough cross-bedded, massive and Gilbert-type foreset lithofacies. Contacts between siltstone and high-flow regime planar parallel and wavy parallel lithofacies, however, are conformable. Similar lacustrine deltaic sequences have been described in the Laney Member (Stanley

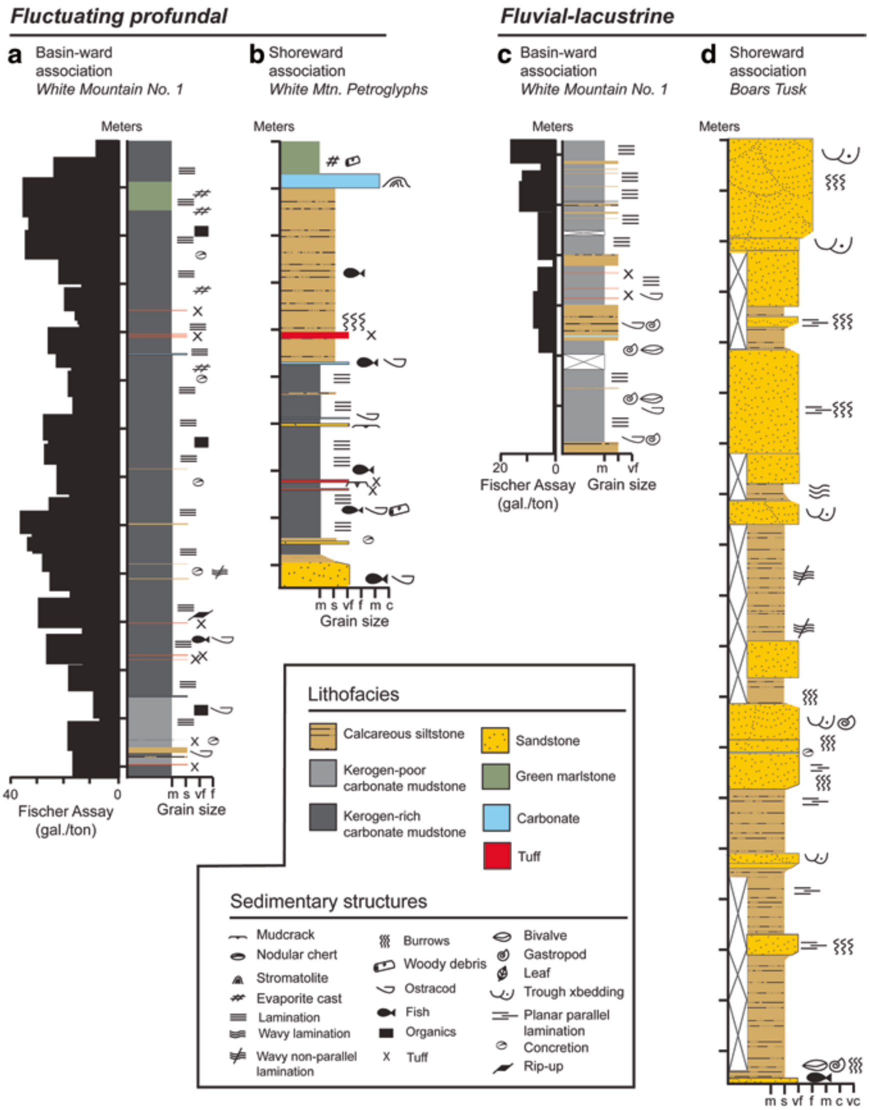

Fig. 3.5 Representative stratigraphic sections from the four principle lithofacies associations: The fluvial-lacustrine lithofacies assemblage has distinct (**a**) basin-ward and (**b**) shoreward associations. The basin-ward association is typified by the massive mudstone lithofacies and punctuated by fining upward interbeds of fossil-bearing siltstone lithofacies. Freshwater fauna, such as gastropods and bivalves are abundant throughout. The shoreward association is typified by stacked, coarsening upwards sequences of siltstone and sandstone lithofacies. The fluctuating profundal lithofacies assemblage also has distinct (**c**) basin-ward and (**d**) shoreward associations. The basin-ward association is typified by oscillations between thinly laminated, organic rich mudstone and variably laminated mudstone lithofacies. These oscillations are also apparent in Fischer Assay. The shoreward association is typified by a diverse array of fine-clastic, coarse-clastic, and biogenic lithofacies. Mud-cracked horizons are also observed. Well-preserved fish are common throughout both associations

and Surdam 1978), Lake Bonneville (Lemons and Chan 1999) and in the East Gobi Basin (Johnson and Graham 2004). The progradational and aggradational geometries of the sandstones suggest sustained sediment influx, while rip-ups and irregular lithofacies contacts indicate infrequent storm generated high-flow and erosive hydrologic conditions.

3.4.2 Fluctuating Profundal Lithofacies Assemblage

Basin-ward association The association is characterized predominantly by kerogen-rich, commonly fish fossil-bearing mudstone lithofacies (Fig. 3.5c), with minor interlaminations of fossiliferous siltstone and, less commonly, ostracode and ooid grainstone. The increased preservation of intact fish fossils and absence of benthos within this assemblage relative to that observed within the fluvial-lacustrine assemblage indicates increased chemical and thermal stratification and the presence of anoxic water bottoms. Moreover, the absence of bivalves suggests lake waters of this assemblage were more saline than those of the fluvial-lacustrine assemblage, where bivalves were abundant.

In detail, basin-ward association of the fluctuating profundal assemblage is characterized by alternating intervals of both massive and microlaminated kerogen-rich mudstone and less organic-rich mudstone lithofacies (Fig. 3.5c). These facies alternations are apparent in Fischer Assay logs of oil yield, and are interpreted to represent oscillations between low- and high-stand conditions within a hydrologically closed lake system. Specifically, laminated, organic-rich and massive organic-rich mudstone correspond to high-stand lake conditions, when lake level was at a maximum and clastic dilution at a minimum. During these conditions, cold, freshwater input flows over denser, more saline resident lake waters amplified the chemical and thermal stratification within the lake system. The corresponding increase in oxygenation and nutrient delivery results in increased production of particulate organics, which were preserved in the anoxic bottom waters. Less organic-rich mudstone intervals in turn correspond to low-stand lake conditions, when water input is decreased relative to high-stand conditions. Stratification, as well as oxygen and nutrient delivery was correspondingly suppressed by a reduction of freshwater input, resulting in a decrease in both the production and ultimate preservation of particulate organics.

Shoreward association A diverse array of successive, interbedded fine- and coarse-clastic sediments within the Rife bed typifies the shoreward association of the fluctuating profundal assemblage (Fig. 3.5d). Laminated organic-rich mudstone, massive organic-rich mudstone and, to a lesser extent, variably laminated mudstone lithofacies are interlaminated by thin (<20 cm) packages of ostracode and oolitic grainstone, stromatolite, and massive sandstone lithofacies. Meter-scale intervals of massive sandstone and fossil-bearing siltstone are observed in the north central to northern-most field sections and are thought to represent closer proximity to lake margins. In both the WMP and BT field sections, stromatolites overlie large packages of fish and ostracode-bearing fossiliferous siltstone. At BT these stromatolites constitute a 2 m interval. Woody debris, burrows, ostracode molds, and fish debris are common throughout all facies within this association.

Like the basin-ward expression of this assemblage, the absence of freshwater fauna and progradational geometries suggests a relative reduction in sediment and water input when compared to the fluvial-lacustrine assemblage. Facies diversity among this association is also thought to reflect periods of high- and low-stands within the lake system, with fine-grained and bio-clastic sediments reflecting low-stand deposits and pulses of coarse-grained clastics representative of shifts towards high-stand conditions. These oscillations indicate rapid, basin-wide alteration in sediment deposition, organic production, and stratification within the lake-system

3.5 Basin-Scale Stratigraphy

Figure 3.6 illustrates the basin-scale packaging of the Tipton Member, which records three vertical oscillations between fluvial-lacustrine and fluctuating profundal lithofacies. Deltaic sandstone bodies (Farson Sandstone) accumulated at the northern edge of the basin during fluvial-lacustrine intervals, but are largely absent within fluctuating profundal intervals. Within the Tipton

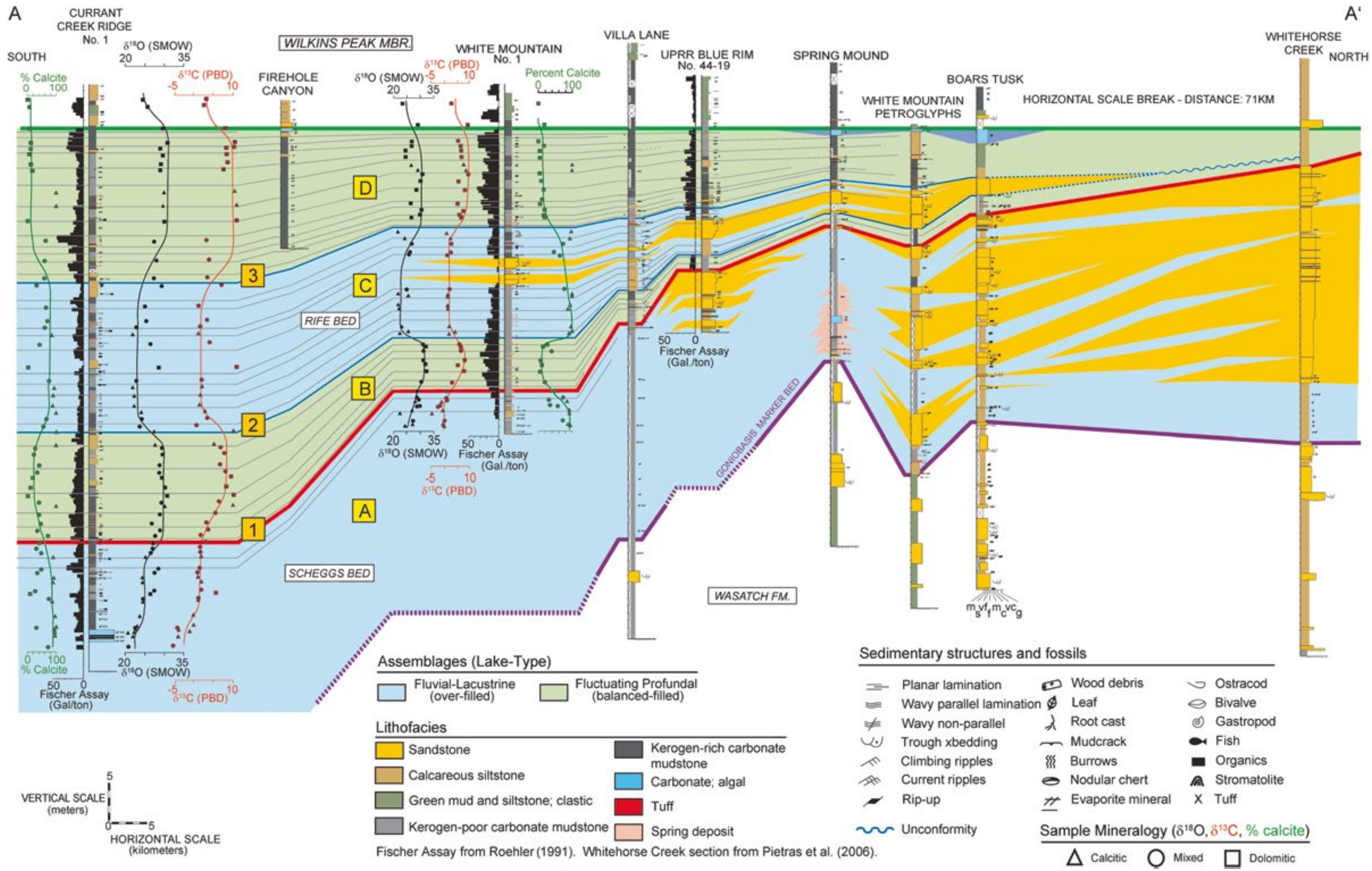

Fig. 3.6 Basin-scale cross-section of the Tipton Member west of the Rock Springs Uplift in the Green River Basin, Wyoming. From south (A) to north (A′), these sections are Currant Creek Ridge Core No. 1 (CCR), Firehole Canyon (FC), White Mountain Core No. 1 (WM1), Villa Lane (VL), UPRR Blue Rim 44-19 core (BR), Spring Mound (SM), White Mountain Petroglyphs (WMP), Boar's Tusk (BT), and Whitehorse Creek (WC). [Fischer Assay data modified from Roehler (1991a), and Whitehorse Creek (WC) field section modified from Pietras (2003)]. See Walker (2008) for complete stratigraphic dataset

Member, transitions between lithofacies assemblages are gradational, particularly in basin-ward locations. Because the basin-ward expressions of both assemblages share multiple lithofacies, transitions lack distinct lithologic contrast. Basin-ward transitions are, therefore, constrained primarily on the basis of relative organic-content (fluctuating profundal lithofacies exhibit higher Fischer Assay oil yield) and the presence or absence of freshwater bivalves. The appearance of fossil fish at the base of the Laney Member indicates the transition from a hydrologically closed lake system to a partly open system with fresh surface water (Carroll and Bohacs 1999; Rhodes 2002). Fish remains are preserved within all lake-type assemblages of the Tipton Member, and similarly indicate that conditions, at least the uppermost lake water, were fresh. It should be noted, however, that intact fossils are more common in the fluctuating profundal assemblage, while fish "debris", a slurry of bones, scales, and fins, is most common, though not restricted to, the fluvial-lacustrine assemblage. Though lithologic transitions also appear gradational at basin margins, they are marked by stronger lithologic contrasts. The contact from fluvial-lacustrine to fluctuating profundal assemblage, for example, is placed at the top of large bodies of prograding, coarse-clastic lithofacies and the initiation of profundal mudstone deposition.

3.5.1 Correlations

Correlation of the upper and lower limits of the Tipton Member was established using lithofacies assemblages, and is supported by Fischer Assay (Roehler 1991a), geochemical, and XRD analyses of CCR and WM cores (Fig. 3.6). Due to limited core and outcrop in the southern area of the basin, direct observation of the Wasatch Formation-Tipton Member contact was limited to field sections in the northern part of the basin (VL, SM, WMP, BT, and WC). Where observed, the contact is defined where oxidized (red) and reduced (green) fluvial plain siltstone and mudstone of the Wasatch Formation transition to gastropod-bearing mudstone and siltstone lithofacies of the Scheggs bed. This fossiliferous horizon is often referred to in literature as the *Goniobasis* Marker bed, as the horizon contains abundant *Goniobasis tenera* gastropods (Hanley 1976).

Previous analysis of the Tipton Member (Roehler 1991b) defined the Scheggs-Rife contact at the transition from freshwater, calcitic deposits to saline, dolomitic deposits. This study adheres to that previous terminology, placing the Scheggs-Rife contact at the first transition from a fluvial-lacustrine lithofacies assemblage (freshwater) to a fluctuating-profundal assemblage (more saline). This stratigraphic placement of the Scheggs-Rife contact coincides with a 56 % average decrease in calcite content and a gradual increase in $\delta^{18}O$ and $\delta^{13}C$ values (Fig. 3.6).

In the northern part of the basin (Fig. 3.6), the top of the Rife bed is characterized by stromatolite lithofacies (.25–1.5 m thick). These beds are conformably overlain by green, marcesite- and pyrite-bearing, mud-cracked mudstone and siltstone lithofacies of the Wilkins Peak Member. In the central and southern part of the GGRB, the Tipton Member-Wilkins Peak Member contact is defined where mm- and cm-laminated mudstone lithofacies of the Rife bed gradually transition to evaporative lithofacies of the Wilkins Peak Member. Within this study, the basin-ward and shore-ward expressions of the Tipton Member-Wilkins Peak Member contact are conformable, and coincide with a subtle isotopic trend towards lighter $\delta^{18}O$ and $\delta^{13}C$ values, as well as a sharp reduction in Fischer Assay oil yield, which is sustained at 0 gal./ton over a 1 m interval (Roehler 1991a). The conformable interpretation of the Tipton Member-Wilkins Peak Member contact presented by this study is somewhat discordant with that presented by Pietras et al. (2003), who propose that a major sequence boundary defines the contact. We argue instead that the Tipton-Wilkins Peak contact records a sharp change in water chemistry and brief subaeriel exposure of the edges of the basin, but not necessarily a basin-wide major lacuna.

3.6 Stable Isotope Analysis

Oxygen isotopes Stable isotopic analysis of profundal mudstone from two cores, CCR and WM, distinguish four distinct $\delta^{18}O$ zones within the Tipton Member (Table 3.3). These intervals directly correlate with zones defined by lithofacies assemblages. Fluvial-lacustrine Zones A and C have light $\delta^{18}O$ values (25.3‰ and 23.0‰, respectively), while fluctuating profundal Zones B and D exhibit the heaviest $\delta^{18}O$ signature within the Tipton Member (29.7‰ and 29.8‰, respectively). The $\delta^{18}O$ transition from Zone A to Zone B (Shift 1) occurs gradually over 4 m within both CCR and WM cores. The transition from Zone B to Zone C (Shift 2), however, is abrupt, occurring over a 2 m interval. Because Zones C and D are under-sampled in both CCR and WM cores, the transition interval of Shift 3 cannot accurately be assessed.

Carbon isotopes The $\delta^{13}C$ signature of the Tipton Member exhibits four distinct zones, all of which are coincident and directly correlative with those observed within the $\delta^{18}O$ profiles of the same cores (Fig. 3.6; Table 3.3). Like the $\delta^{18}O$ profile of the Tipton Member, $\delta^{13}C$ is heaviest in fluctuating profundal Zones B and D (5.3‰ and 8.5‰, respectively). Fluvial-lacustrine Zones A and C have relatively lighter $\delta^{13}C$ values at 0.6‰ and 1.9‰, respectively. Because carbon isotopic data was obtained from the same samples as $\delta^{18}O$ values, the isotopic transition intervals and trends of the $\delta^{13}C$ signature within the Tipton Member is the same as that of the $\delta^{18}O$ profile.

$\delta^{18}O$ and $\delta^{13}C$ covariance Among profundal mudstone samples of the Tipton Member, correlation between $\delta^{18}O$ and $\delta^{13}C$ is generally moderate. Correlation is notably stronger within all samples of the CCR core ($R^2=0.7292$, $n=26$) than it is among those within the WM core (Fig. 3.7a). $\delta^{18}O$ and $\delta^{13}C$ correlation among samples sharing distinct carbonate mineralogy is also strongest in the CCR core (Fig. 3.7b). Dolomitic samples within the CCR core, for example, exhibit a stronger correlation ($R^2=0.9062$, $n=6$) than dolomitic samples within the WM core ($R^2=0.0250$, $n=10$). Moreover, while dolomitic samples have the strongest $\delta^{18}O$ and $\delta^{13}C$ correlation compared to other carbonate mineralogies within CCR core, calcitic samples are the most strongly correlated within the WM core ($R^2=0.3122$, $n=8$). This suggests that carbonate mineralogy does not influence $\delta^{18}O$ and $\delta^{13}C$ correlation in a predictable way across the basin. Among both core, fluctuating profundal zones exhibit stronger overall $\delta^{18}O$ and $\delta^{13}C$ correlation ($R^2=0.2392$, $n=18$) than do fluvial-lacustrine zones ($R^2=0.0835$, $n=33$) (Fig. 3.7c).

3.7 Discussion

3.7.1 Stratigraphic Evolution

Major changes in Tipton Member lacustrine lithofacies were closely associated with initiations and cessations of Farson Sandstone deposition, suggesting that changes of fluvial influx into the basin were a primary driver. Within

Table 3.3 Average Zonal Tipton Member Geochemistry, mineralogy and oil yield

Zone	n	$\delta^{18}O^a$ (VSMOW)	±1σ	$\delta^{13}C^a$ (VPDB)	±1σ	% calcite[a]	±1σ	Oil yield (Gal./ton)[b]
D	5	29.8	1.7	8.5	1.9	12.0	5.3	19.2
C	*5*	*23.0*	*1.6*	*1.9*	*0.3*	*80.1*	*12.5*	*9.7*
B	13	29.7	1.6	5.3	2.2	30.4	18.4	17.6
A	*25*	*25.3*	*2.4*	*0.6*	*2.4*	*69.1*	*27.3*	*7.6*

Notes: Italicized rows represent fluvial-lacustrine lithofacies assemblages, non-italicized rows represent fluctuating profundal lithofacies assemblages
[a]Average among CCR and WM cores
[b]Thickness-weighted average oil yield from Fischer Assay of CCR and WM cores (Roehler 1991a)

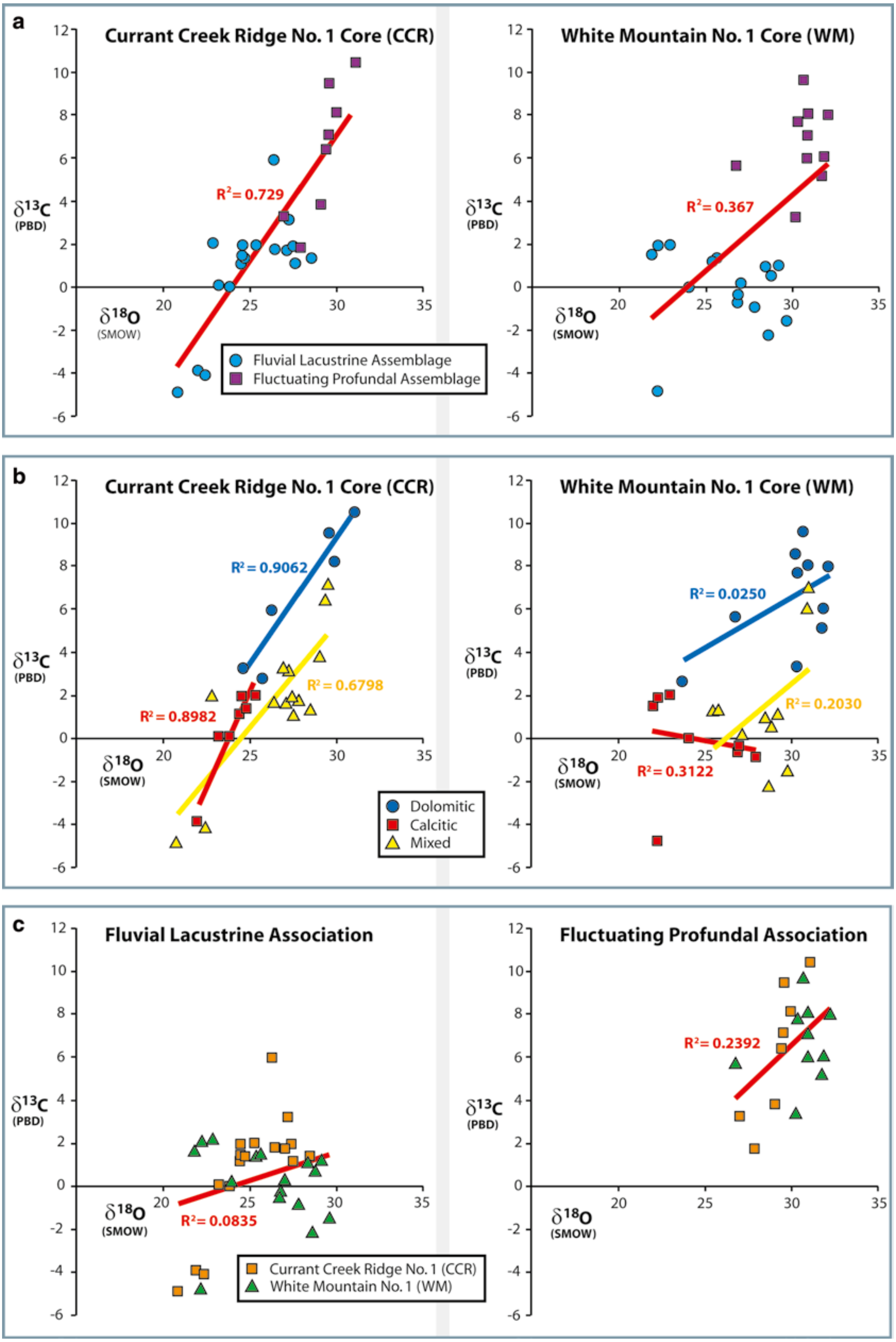

Fig. 3.7 The δ18O and δ13C covariance among litho-stratigraphic intervals of (**a**) CCR and WM cores, (**b**) carbonate mineralogy of samples within CCR and WM cores, and (**c**) within each litho-stratigraphic zone

fluvial-lacustrine Zones A and C, progradational geometries along the lake margin indicate significant sediment and, thus, fluvial input into a hydrologically open (i.e. overflowing) lake basin. The Farson Sandstone is not observed within Zones B and D, indicating a relative reduction in sediment/fluvial input during fluctuating profundal deposition. With continuing tectonic subsidence in the basin and the absence of the high sediment input, accommodation was increased in fluctuating profundal Zones B and D. Reflecting this, lake margins transgressed and reach their maximum extent (Fig. 3.6). Additionally, prograding stratal geometries of fluvial-lacustrine intervals are replaced by aggradation of sediment in Zones B and D, indicating a transition to a hydrologically closed (i.e. impounded) lake basin. Carroll and Bohacs (1999) define three lake types, overfilled, balanced-filled, and underfilled, that are controlled by the amount of water and sediment input relative to basin accommodation. Using this lake-type characterization, fluvial-lacustrine intervals of the Tipton Member are classified as overfilled, while fluctuating profundal intervals are balanced-filled.

Distinct zones of carbonate mineralogy and Fischer Assay oil yield coincide with the lithologically defined intervals. Fluvial-lacustrine intervals A and C are relatively calcitic, exhibiting 75 % calcite on average. These intervals are generally poor in organic matter, with a weighted average Fischer Assay oil yield of 8.7 gal./ton, suggesting that well-oxygenated, unstratified lake conditions were present during deposition. Low oil yields can result from clastic dilution resulting from sustained fluvial input of siliciclastic detritus into an open lake system (Bohacs et al. 2000; Carroll and Bohacs 2001).

In contrast, fluctuating profundal intervals are relatively dolomitic, exhibiting 21 % calcite on average. The presence of dolomite within the Tipton Member can be explained via the biogenic model of Desborough (1978), whereby Mg is preferentially concentrated along lake bottoms as blue-green algae anaerobically decompose. Supporting this model is relatively high Fischer Assay oil yield (18 gal./ton) among profundal deposits of fluctuating profundal intervals. Alternatively, the playa lake model is commonly applied to the GRF to explain dolomite generation and distribution (Eugster and Surdam 1973; Mason and Surdam 1992). However, its application to the Tipton Member is inappropriate due to a lack of playa indicators (e.g. evaporite mineral casts, large scale desiccation features).

3.7.2 Isotopic Evolution

Diagenesis Though post-lithification diagenesis can alter stable isotopic composition (Morrill and Koch 2002), our study observes several characteristics in both the lithology and geography of the study area that suggest the isotopic signature of the Tipton Member reflects the composition of Lake Gosiute during deposition.

Because aragonite is highly susceptible to diagenic alteration, its presence or absence can be used as a proxy for diagenic evaluation. Aragonitic bivalves were recovered from Zone A in the CCR core. Preserved growth bands within these shells, which would have been destroyed by diagenic alteration, suggest diagenesis had not occurred within surrounding sediments. Moreover, the mean $\delta^{18}O$ and $\delta^{13}C$ values of these bivalves (21.98‰ and −3.86‰, respectively) are lower than other light values recorded throughout the Tipton Member. Because aragonitic samples are interpreted to have been unaltered, similarly light $\delta^{18}O$ and $\delta^{13}C$ values within the Tipton Member are believed to reflect primary depositional conditions.

Profundal mudstone of the Tipton Member is relatively fine-grained and impermeable, a characteristic which inhibits the pervasiveness of diagenic solutions. Coquina interbeds within the CCR core best exhibit this impermeability. Preservation of primary aragonite is limited to matrix-supported interbeds, whereas clast- (i.e. shell-) supported interbeds are calcified. This suggests profundal mudstone is an effective shield against diagenic solutions.

The spatial distribution of isotopic trends themselves also suggests that alteration of $\delta^{18}O$ and $\delta^{13}C$ values is unlikely. Specifically, the same isotopic pattern is observed in CCR and WM cores, which are separated by over 65 km, a distance unlikely to be transversed by a homogenous diagenic solution. In order to create four, isotopically distinct zones, diagenic solutions would have had to occur with variable intensities along multiple, vertically spaced horizons. Furthermore, if diagenesis were responsible for each zone, the shift from isotopically heavy Zone B to isotopically light Zone C (Shift 2) would indicate more intense diagenic alteration up-section, an event that is highly unlikely.

Mineralogical effects on $\delta^{18}O$ Because carbonate minerals exhibit differential fractionation at surface temperatures (Sharma and Clayton 1965; Fritz and Smith 1970; Rosenbaum and Sheppard 1986), sample mineralogy can also compromise $\delta^{18}O$ analysis. Dolomite, for example, is inferred to have a 3‰ heavier $\delta^{18}O$ value than calcite precipitated from the same water (Fritz and Smith 1970). The isotopic shifts within the Tipton Member involve calcitic, mixed, and dolomitic mineralogy. As such it is possible that differential fractionation among distinct carbonate mineralogies may influence the $\delta^{18}O$ signatures within the Tipton Member. However, in several shifts (i.e. Shift 1, Shift 2), the trends towards heavier or lighter isotopic values are preserved within the individual trend of each carbonate classification (e.g. calcite, mixed, and dolomitic). Therefore, while mineralogy may influence the magnitude of each isotopic shift, this observation suggests that shifts within the Tipton Member reflect major changes in lake water chemistry during deposition. Furthermore, covariance among mineralogy and $\delta^{18}O$ results is insignificant among all carbonate mineralogies, with R^2 correlation values of 0.1043 (dominantly dolomitic samples), 0.2146 (dominantly calcitic samples), and 0.4263 (mixed samples) (Fig. 3.8).

Effects on $\delta^{18}O$ and $\delta^{13}C$ and their implications The variable $\delta^{18}O$ signature observed within the Tipton Member is likely related to the combined effects of continued evaporation and variable residence time of lake waters. Evaporation preferentially removes $\delta^{16}O$ from surface waters, thereby concentrating $\delta^{18}O$ within a lake system. Increased residence time of lake waters within a lake basin compounds these evaporative effects, resulting in heavier $\delta^{18}O$ values. Because lake water within a hydrologically closed lake system experiences longer residence time and, thus, exhibits heavier $\delta^{18}O$ values, the

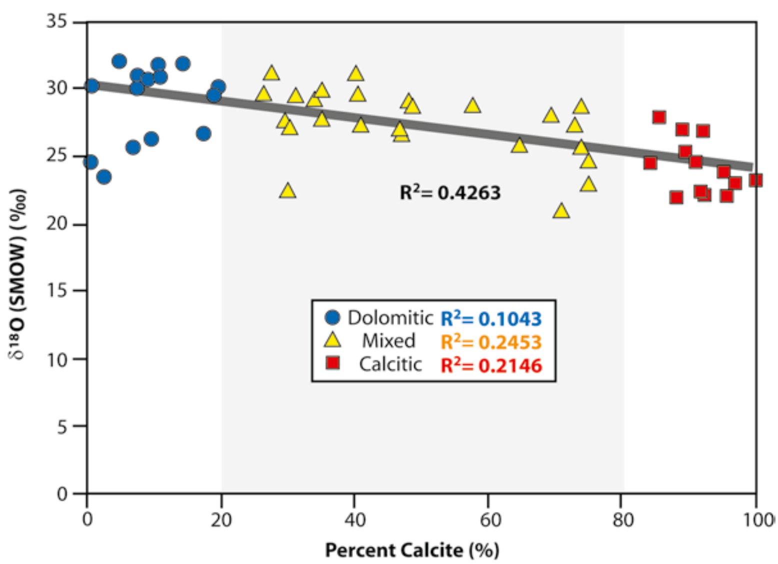

Fig. 3.8 Comparison of mineralogy and $\delta^{18}O$ composition within the Tipton Member. Calcitic samples exhibit the lowest $\delta^{18}O$ values, while dolomitic samples exhibit the highest $\delta^{18}O$ values

heavy isotopic signature of fluctuating profundal zones B and D of the Tipton Member are interpreted to reflect closed lake conditions. Lighter $\delta^{18}O$ values of Zones A and C indicate open lake conditions during fluvial-lacustrine deposition.

The $\delta^{13}C$ signature of lacustrine deposits is generally more complex, as it is related to the rate of primary productivity (Kirby et al. 2002), the rate of organic decomposition within the lake system (Pitman 1996), and dissolved inorganic carbon (DIC) input from Phanerozoic limestone in Lake Gosiute's catchment ($\delta^{13}C \approx 0$). Photosynthetic algae preferentially remove $\delta^{12}C$ throughout their lifetime, thereby enriching lake waters in $\delta^{13}C$ if they are buried prior to decomposition. In this way, higher inorganic $\delta^{13}C$ values reflect periods of abundant productivity, while lower $\delta^{13}C$ values indicate depositional periods that are less conducive to organic production. Deposits within fluctuating profundal Zones B and D have higher $\delta^{13}C$ (5.33‰ and 8.5‰, respectively) compared to fluvial-lacustrine Zones A and B (0.648 and 1.88‰) and are, therefore, interpreted to have supported higher rates of primary productivity.

Fischer Assay of balanced-filled and overfilled zones supports a primary productivity interpretation of $\delta^{13}C$ results. In those zones having higher concentrations of $\delta^{13}C$, increased Fischer Assay values correspond. Zones B and D have an average Fischer Assay value of 17.6 Gal./ton and 19.2 Gal./ton, respectively. Comparatively, Zones A and C, which have lower $\delta^{13}C$ values, exhibit significantly lower Fischer Assay measures of organic content at 7.6 Gal./ton and 9.7 Gal./ton, respectively.

Another possible influence on the $\delta^{13}C$ profile across the Tipton Member is the rate at which particulate organics decompose within the lake system. As organic material decomposes, $\delta^{12}C$ is released into the lake waters by methanogenesis, thereby decreasing the $\delta^{13}C$ values recorded by sediments (Pitman 1996). Consequently, low $\delta^{13}C$ may be used as a proxy to evaluate the extent to which lake waters were chemically and thermally stratified. Decomposition of organic matter is reduced if not stopped entirely within a stratified lake system. Within anoxic conditions of a stratified lake system, less $\delta^{12}C$ would be available to dilute $\delta^{13}C$ concentrations within the stratified lake. In this way, fluctuating profundal Zones B and D reflect periods of well-stratified lake waters. Low $\delta^{13}C$ values within fluvial-lacustrine Zones A and C contrarily reflect less-stratified lake waters.

Carbon inputs from limestone bedrock ($\delta^{13}C \approx 0$) can also lower the $\delta^{13}C$ value of lake sediments. Lower Phanerozoic sections surrounding the GGRB are carbonate, and marginal conglomerates include limestone and dolostone clasts. Though these may have influenced the $\delta^{13}C$ signature of the Tipton Member, the modeling of profundal deposits of the Laney Member (Doebbert 2006; Doebbert et al. 2010) indicates such an effect could not produce $\delta^{13}C$ shifts observed in the GGRB.

Correlation between $\delta^{18}O$ and $\delta^{13}C$ values is often interpreted as a reflection of hydrologically closed lakes because of increased residence time of lake waters (Talbot 1990; Pitman et al. 1996) and successive, rapid lake volume oscillations (Li and Ku 1997). These observations coincide with correlation trends observed among intervals of the Tipton Member, where balanced-filled (i.e. closed lake-basin) deposits of fluctuating profundal intervals (Zones B and D) have a stronger correlation ($R^2 = 0.2392$) than overfilled (i.e. open lake-basin) deposits of fluvial-lacustrine Zones A and C ($R^2 = 0.0835$) (Fig. 3.7c).

3.7.3 Possible Origins of Isotopic and Lake Type Variation

Long-term variation in the rates of precipitation and evaporation are one possible explanation for variation in $\delta^{18}O$ values of lake sediments, and would likely have varied following orbital changes to summer insolation (Morrill et al. 2001). The pace and magnitude of isotopic variation within the Tipton Member is difficult to relate to climate oscillations. In order to produce the dramatic $\delta^{18}O$ shifts observed within the Tipton Member, temperatures would have had to have oscillated between extreme values during the Eocene. The Paleocene-Eocene Thermal

Maximum (PETM) in the Bighorn Basin for example is marked by a 2‰ shift in $\delta^{18}O$ (Koch et al. 2003), and has been associated with a 4–6 °C temperature increase within the western United States (Fricke et al. 1999; Fricke and Wing 2004), as well as a global sea surface warming of 8 °C (Zachos et al. 2001, 2008). To produce the 4.46‰, 6.68‰, and 7.64‰ $\delta^{18}O$ shifts recorded within the Tipton Member (Shifts 1, 2, and 3, respectively), temperature change during Tipton deposition would have been pronounced, rapid in onset, and persistent, and have no clear corollary, in the marine record Westerhold and Röhl (2009). Existing geochronology (Smith et al. 2008, 2010) constrains Rife bed deposition to 0.60 ± 0.31 m.y. (2σ). Assuming all three lithostratigraphic zones within the Rife bed (zones B, C, and D) were deposited in approximately the same amount of time, each would represent ca. 200 k.y., and may potentially coincide with orbital eccentricity variations.

The lithofacies, aerial extent, and $\delta^{18}O$ characteristics of the two different lake types make is difficult, however to relate isotopic changes to climate parameters. Following the evaporation-driven hypothesis, during increased periods of evaporation, lake level should have diminished, subaerially exposing broad areas of the lake margin, which would have in turn led to evaporative concentration of ^{18}O in lake waters, which is inconsistent with lithofacies-based observations of high lake level during deposition of $\delta^{18}O$-heavy zones B and D (Figs. 3.6 and 3.9). These fluctuating profundal zones consist largely of deep lake deposits that lack evidence for systematic desiccation and consistently overlie shallower-water lithofacies of underlying fluvial-lacustrine zones A and C.

Diversions of upstream drainage provides an appealing solution to the apparent paradox of high lake level and high $\delta^{18}O$ composition observed in the Tipton Member. In such a scenario, abrupt changes to regional hydrology and isotopic composition would have been triggered by the inclusion or exclusion of a source of light $\delta^{18}O$-depleted waters and sediment delivered from an upland source (e.g., Carroll et al 2008). In our preferred model for the lake-type shifts observed within the Tipton Member (Fig. 3.9),

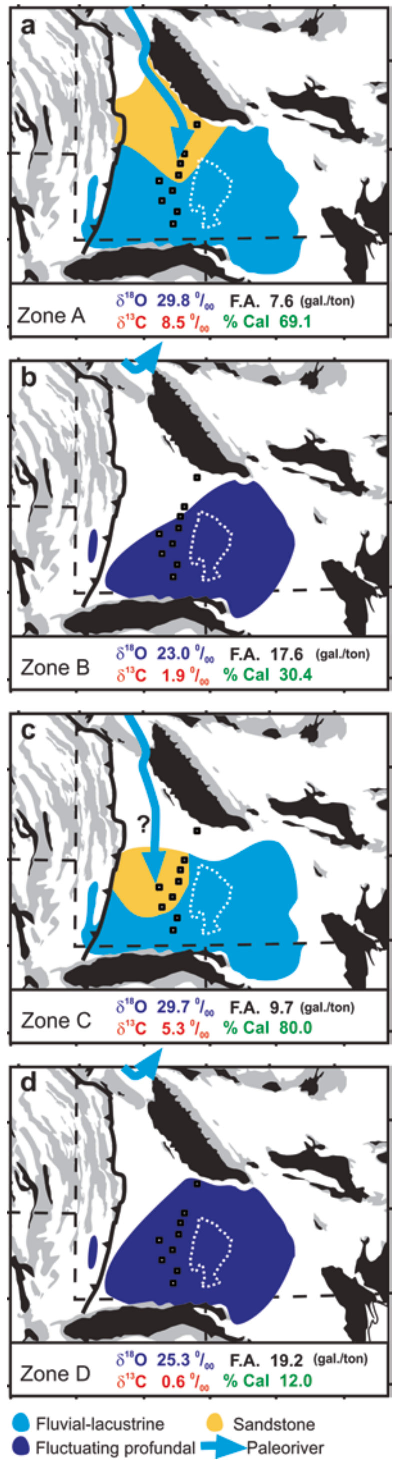

Fig. 3.9 Interpreted four part synoptic lake type evolution of the Tipton Member. A major water and sediment source entered the GGRB during fluvial lacustrine deposition (zones A and C), and was diverted away from the basin during fluctuating profundal deposition (zones B and D)

Shift 1 is attributed to diversion of such a stream, followed by its recapture (Shift 2) and ultimate diversion (Shift 3). With each drainage diversion event, deposition of the Farson Sandstone ceased, accommodation increased in the absence of sediment input within the basin center, and lake margins correspondingly transgressed. Removal of a low $\delta^{18}O$ hydrologic source and the associated increase in lake water residence time due to the lowered hydrologic throughput would both have acted to elevate the $\delta^{18}O$ composition of Lake Gosiute. Doebbert et al. (2010) interpreted a similar magnitude $\delta^{18}O$ and provenance shift in the Laney Member of the Green River Formation to have been triggered by the capture of a hinterland sourced stream. They interpreted it to be the terminus of a series of paleovalleys mapped by Janecke et al. (2000), the "Idaho River". Though precise paleotopography of the upstream fluvial network(s) that triggered Tipton Member lake-type reorganizations is not certain, the location of its entry point in the northwest corner of the Greater Green River Basin, the areal distribution and progradation direction of the Farson Sandstone, and the presence of hinterland-sourced quartzite cobbles to the alluvial Pass Peak Formation (Smith et al. 2008) suggest strong similarities between the stream the fed Gosiute during zones A and C of the Tipton and the aforementioned Idaho River. The river in question would have likely have utilized a narrow pathway between the Wind River and Teton-Gros Ventre uplifts in the northern part of the GGRB, but would have delivered far less volcaniclastic detritus to Lake Gosiute because it predated the main phase of Challis volcanism (Smith et al. 2008). The ultimate cause for particular avulsions and captures remains enigmatic. Some could have been triggered by episodic faulting at upstream pathways between growing geologic structures within the drainage network or alternatively some could have occurred in an entirely autogenic fashion due to stream processes. In either case, any successful paleogeomorphic model for Tipton Member must account for the avulsion, return, and subsequent avulsion of this (or another) fluvial source to the basin during its deposition.

3.8 Conclusions

1. Thirteen distinct lithofacies occur within the Tipton Member and comprise two lithofacies assemblages: fluvial-lacustrine and fluctuating profundal, both of which have distinct basin-ward and shoreward expressions.
2. The Scheggs-Rife contact coincides with the first transition from fluvial-lacustrine (overfilled) to fluctuating profundal (balanced-filled) deposits.
3. Though lithostratigraphic transitions between profundal assemblages are subtle, distinct mineralogical, stable isotopic, and Fischer Assay oil yield values delineate abrupt lake system transitions.
4. Fluvial-lacustrine (overfilled) intervals exhibit prograding stratal geometries, dominantly calcitic carbonate mineralogy, low Fischer Assay oil yield, and light $\delta^{18}O$ and $\delta^{13}C$ values. Deposition is interpreted to have occurred within an open lake basin.
5. Fluctuating profundal (balanced-filled) intervals are defined by vertically aggrading stratigraphic geometries, dominantly dolomitic carbonate mineralogy, high Fischer Assay oil yield, and heavy $\delta^{18}O$ and $\delta^{13}C$ values. Deposition is interpreted to have occurred within an intermittently-closed lake basin.
6. Contrary to previous interpretations, the Rife bed contains both fluvial-lacustrine and fluctuating profundal intervals. The lower Rife bed is characterized by fluctuating profundal deposits, the middle Rife bed by fluvial-lacustrine deposits, while the upper Rife bed exhibits fluctuating profundal deposits.
7. In the northern GGRB, the Farson Sandstone is a lateral equivalent of both the Scheggs bed and zone C of the overlying Rife bed, and is thus constrained to fluvial-lacustrine intervals.
8. Oscillating lithologic and stable isotopic signatures within the Tipton Member are thought to reflect paleohydrologic reorganizations of the Farson Sandstone-sourcing fluvial system. Specifically, a diversion, recapture and ultimate diversion of this source are thought to have resulted in Shifts 1, 2 and 3.

9. Two possible mechanisms for paleohydrologic reorganization are proposed: episodic faulting or uplift upstream of the basin; and dynamic geomorphology of the Farson Sandstone-sourcing river itself. In both instances, a major fluvial source is diverted outside of the GGRB.

Acknowledgments This study was assisted by discussions with Shanan Peters, Amalia Doebbert, Eric Williams. Lisa Lesar was a courageous assistant in the field. We thank the staff at the U.S.G.S. Core Repository in Denver, Colorado for use of their facility and intimate knowledge of available core. Jason Huberty assisted acquisition of XRD analyses. We thank the American Association of Petroleum Geologists, ConocoPhillips and the Department of Geology and Geophysics at the University of Wisconsin-Madison for their financial support.

References

Allen JRL (1962) Asymmetrical ripple marks and the origin of cross-stratification. Nature 194:84–115

Allen JRL (1982) Sedimentary structures: their character and physical basis, vol 30, Developments in sedimentology. Elsevier, Amsterdam

Arnott RW (1993) Quasi-planar-laminated sandstone beds of the Lower Cretaceous Bootlegger Member, north-central Montana; evidence of combined-flow sedimentation. J Sediment Petrol 63:488–494

Arnott RW, Southard JB (1990) Exploratory flow-duct experiments on combined-flow bed configurations, and some implications for interpreting storm-event stratification. J Sediment Petrol 60:211–219

Balch DP, Cohen AS, Schnurrenberger DW, Haskell BJ, Valero Garces BL, Beck JW, Cheng H, Edwards RL (2005) Ecosystem and paleohydrological response to Quaternary climate change in the Bonneville Basin, Utah. Palaeogeogr Palaeoclimatol Palaeoecol 221:99–122

Bohacs KM (1998) Contrasting expressions of depositional sequences in mudrocks from marine to nonmarine environs. In: Schieber J, Zimmerlie W, Sethi P (eds) Mudstones and shales, vol 1, Characteristics at the basin scale. Schweizerbart'sche Verlagsbuchhandlung, Stuttgart, pp 32–77

Bohacs KM, Carroll AR, Neal JE, Mankiewicz PJ (2000) Lake-basin type, source potential, and hydrocarbon character: an integrated sequence-stratigraphic-geochemical framework. In: Gierlowski-Kordesch EH, Kelts KR (eds) Lake basins through space and time, vol 46, American Association of Petroleum Geologists studies in geology. American Association of Petroleum Geologists, Tulsa, pp 3–34

Born SM (1972) Late Quaternary history, deltaic sedimentation, and mud lump formation at Pyramid Lake, Nevada. Center for Water Resources Research, Desert Research Institute, University of Nevada, Reno, p 97

Bradley WH (1929) The varves and climate of the Green River epoch, U.S. Geological Survey professional paper 158-E. U.S. Government Printing Office, Washington, DC, p 110

Bradley WH (1931) Origin and microfossils of the oil shale of the Green River Formation of Colorado and Utah, vol 168, U.S. Geological Survey professional paper. U.S. Government Printing Office, Washington, DC, p 58

Bridge JS (1978) Origin of horizontal lamination under turbulent boundary layers. Sediment Geol 20:1–16

Buchheim HP, Eugster HP (1998) Eocene Fossil Lake: the Green River Formation of Fossil Basin, southwestern Wyoming. In: Pitman JK, Carroll AR (eds) Modern & ancient lake systems; new problems and perspectives, vol 26, Utah Geological Association publication. Utah Geological Association, Salt Lake City, pp 191–208

Buchheim HP, Surdam RC (1977) Fossil catfish and the depositional environment of the Green River Formation, Wyoming. Geology 5:196–198

Carroll AR (1998) Upper Permian lacustrine organic facies evolution, Southern Junggar Basin, NW China. Org Geochem 28:649–667

Carroll AR, Bohacs KM (1999) Stratigraphic classification of ancient lakes: balancing tectonic and climatic controls. Geology 27:99–102

Carroll AR, Bohacs KM (2001) Lake-type controls on petroleum source rock potential in nonmarine basins. Am Assoc Pet Geol Bull 85:1033–1053

Carroll AR, Doebbert AC, Booth AL, Chamberlain CP, Rhodes-Carson MK, Smith ME, Johnson CM, Beard BL (2008) Capture of high-altitude precipitation by a low-altitude Eocene lake, western U.S. Geology 36:791–794

Cassanova J, Hillaire-Marcel C (1992) Late Holocene hydrological history of Lake Tanganyika, East Africa, from isotopic data on fossil stramatolites. Palaeogeogr Palaeoclimatol Palaeoecol 91:35–48

Castro EJ (1962) A subsurface study of the Tipton Member of the Green River Formation west of the Rock Springs Uplift University of Wyoming. M.Sc. thesis, University of Wyoming, 66 p

Cheel RJ (1990) Horizontal lamination and the sequence of bed phases and stratification under upper flow-regime conditions. Sedimentology 37:517–529

Cohen AS (1989) The taphonomy of gastropod shell accumulations in large lakes: an example from Lake Tanganyika, Africa. Paleobiology 15:26–45

Cohen AS (2003) Paleolimnology: the history and evolution of lake systems. Oxford University Press, New York

Cohen AS, Thouin C (1987) Near-shore carbonate deposits in Lake Tanganyika. Geology 15:414–418

Culbertson WC, Smith JW, Trudell LG (1980) Oil shale resources and geology of the Green River Formation in the Green River Basin, Wyoming, vol RI-80/6. U.S. Department of Energy, Laramie Energy Technology Center, Laramie, WY.

Dana GF, Smith JW (1972) Oil yields and stratigraphy of the Green River Formation's Tipton Member at Bureau of Mines sites near Green River, Wyoming. U.S. Department of the Interior, Bureau of Mines report of investigation no. 7681

DeCelles PG (1994) Late Cretaceous-Paleocene synorogenic sedimentation and kinematic history of the Sevier thrust belt, northeast Utah and southwest Wyoming. Geol Soc Am Bull 106:32–56

Demaison DJ, Moore GT (1980) Anoxic environments and oil source bed genesis. AAPG Bull 64:1179–1209

Desborough GA (1978) A biogenic-chemical stratified lake model for the origin of oil shale of the Green River Formation: An alternative to the playa-lake model. Geol Soc Am Bull 89:961–971

Dickinson WR, Klute MA, Hayes MJ, Janecke SU, Lundin ER, McKittrick MA, Olivares MD (1988) Paleogeographic and paleotectonic setting of Laramide sedimentary basins in the central Rocky Mountain region. Geol Soc Am Bull 100:1023–1039

Doebbert AC (2006) Geomorphic controls on lacustrine isotopic compositions: evidence from the Laney Member, Green River Formation (Wyoming). M.Sc. thesis, University of Wisconsin-Madison, 255 p

Doebbert AC, Carroll AR, Mulch A, Chetel LM, Chamberlain CP (2010) Geomorphic controls on lacustrine isotopic compositions: evidence from the Laney Member, Green River Formation, Wyoming. Geol Soc Am Bull 122:236–252

Dumas S, Arnott RWC (2006) Origin of hummocky and swaley cross-stratification: the controlling influence of unidirectional current strength and aggradation rate. Geology 34:1073–1076

Dumas S, Arnott RWC, Southard JB (2005) Experiments on oscillatory flow and combined flow bed forms: implications for interpreting parts of the shallow marine sedimentary record. J Sediment Res 72:501–513

Eggleston JR, Dean WE (1976) Freshwater stromatolitic biotherms in Green Lake, New York. In: Walker MR (ed) Stromatolites. Elsevier, Amsterdam, pp 479–488

Eugster HP, Surdam RC (1973) Depositional environment of the Green River Formation of Wyoming: a preliminary report. Geol Soc Am Bull 84:1115–1120

Fischer AG, Roberts LT (1991) Cyclicity in the Green River Formation (lacustrine Eocene) of Wyoming. J Sediment Petrol 61:1146–1154

Fricke HC, Wing SL (2004) Oxygen isotope and paleobotanical estimates of temperature and d^{18}O-latitude gradient over North America during the Early Eocene. Am J Sci 304:612–635

Fricke HC, Clyde WC, O'Neil JR, Gingerich PD (1999) Evidence for rapid climate change in North America during the latest Palaeocene thermal maximum: Oxygen isotope compositions of biogenic phosphate from the Bighorn Basin (Wyoming). Earth Planet Sci Lett 160:193–208

Fritz P, Smith DGW (1970) The isotopic composition of secondary dolomites. Geochim Cosmochim Acta 34:1161–1173

Halley RB (1976) Textural variation within Great Salt Lake algal mounds. In: Walker MR (ed) Stromatolites. Elsevier, Amsterdam, pp 435–445

Hanley JH (1976) Paleosynecology of nonmarine mollusca from the Green River and Wasatch Formations (Eocene), southwestern Wyoming and northwestern Colorado. In: Scott RW, West RR (eds) Structure and classification of paleocommunities. Dowden, Hutchinson & Ross, Inc, Stroudsburg, pp 235–261

Harms JC, Fahnestock RK (1965) Stratification, bed forms, and flow phenomena (with an example from the Rio Grande). In: Primary sedimentary structures and their hydrodynamic interpretation – a symposium, vol 12, Society of Economic Paleontologists and Mineralogists special publication. Society of Paleontologists and Mineralogists, Tulsa, pp 84–115

Horsfield B, Curry DJ, Bohacs KM, Littke R, Rullkötter J, Schenk HJ, Radke M, Schaefer RG, Carroll AR, Isaksen G, Witte EG (1994) Organic geochemistry of freshwater and alkaline lacustrine sediments in the Green River Formation of the Washakie Basin, Wyoming, U.S.A. Org Geochem 22:415–440

Huc AY, Le Fournier J, Vandenbrouke M, Bessereau G (1990) Northern Lake Tanganyika – an example of organic sedimentation in an anoxic rift lake. In: Katz BJ (ed) Lacustrine basin exploration: case studies and modern analogs, vol 50, American Association of Petroleum Geologists memoir. American Association of Petroleum Geologists, Tulsa, pp 169–185

Janecke SU, VanDenburg CJ, Blankenau JJ, M'Gonigle JW (2000) Long-distance longitudinal transport of gravel across the Cordilleran thrust belt of Montana and Idaho. Geology 28:439–442

Johnson CL, Graham SA (2004) Sedimentology and reservoir architecture of a synrift lacustrine delta, southeastern Mongolia. J Sediment Res 74:770–785

Jopling AV, Walker RG (1968) Morphology and origin of ripple-drift cross-lamination, with examples from the Pleistocene of Massachusetts. J Sediment Petrol 38:971–984

Kelts KR, Hsü KJ (1978) Freshwater carbonate sedimentation. In: Lerman A (ed) Lakes: chemistry, geology, and physics. Springer, Berlin, pp 295–323

Kirby ME, Mullins HT, Patterson WP (2002) Late glacial-Holocene atmospheric circulation and precipitation in the northeast United States inferred from modern calibrated stable oxygen and carbon isotopes. Geol Soc Am Bull 114:1326–1340

Kneller B, Buckee C (2000) The structure and fluid mechanics of turbidity currents: a review of some recent studies and their geological implications. Sedimentology 47:62–94

Koch PL, Clyde WC, Hepple RP, Fogel ML, Wing SL, Zachos JC (2003) Carbon and oxygen isotope records from paleosols spanning the Paleocene-Eocene boundary, Bighorn Basin, Wyoming. In: Wing SL, Gingerich PD, Schmitz B, Thomas E (eds) Causes and consequences of globally warm climates in the early paleogene, vol 369, Geological Society of America special paper. Geological Society of America, Boulder, pp 49–64

Leckie DA, Krystinik LF (1989) Is there evidence for geostrophic current preserved in the sedimentary record of inner to middle-shelf deposits? J Sediment Res 59:862–870

Lemons DR, Chan MA (1999) Facies architecture and sequence stratigraphy of fine-grained lacustrine deltas along the eastern margin of Lake Pleistocene Lake Bonneville, northern Utah and southern Idaho. Am Assoc Pet Geol Bull 83:635–665

Li HC, Ku TL (1997) δ^{13}C-δ^{18}O covariance as a paleohydrological indicator for closed-basin lakes. Palaeogeogr Palaeoclimatol Palaeoecol 133:69–80

Mason GM, Surdam RC (1992) Carbonate mineral distribution and isotope fractionation: an approach to depositional environment interpretation, Green River Formation, Wyoming, U.S.A. Chem Geol 101:311–321

McLane M (1995) Sedimentology. Oxford University Press, New York

Morrill C, Koch PL (2002) Elevation or alteration? Evaluation of isotopic constraints on paleoaltitudes surrounding the Eocene Green River Basin. Geology 30:151–154

Morrill C, Small EE, Sloan LC (2001) Modeling orbital forcing of lake level change: Lake Gosiute (Eocene), North America. Global Planet Change 29:57–76

Müller G (1966) The new Rhine delta in Lake Constance. In: Shirley L (ed) Deltas in their geologic framework. Houston Geological Society, Houston, pp 10–124

Nøttvedt A, Kreisa RD (1987) Model for the combined-flow origin of hummocky cross-stratification. Geology 15:357–361

Oriel SS (1961) Tongues of the Wasatch and Green River Formations, Fort Hill area, Wyoming. U.S. Geological Survey professional paper 424-B, U.S. Government Printing Office, Washington, DC, pp 151–152

Paola C, Wiele SM, Reinhart MA (1989) Upper-regime parallel lamination as the result of turbulent sediment transport and low-amplitude bedforms. Sedimentology 36:47–60

Pasierbiewicz KW, Kotlarczyk J (1997) Flume experiments with fine-grained suspensions, with implications for the origin of mud laminites. J Sediment Res 677:510–513

Pietras JT (2003) High-resolution sequence stratigraphy and strontium isotope geochemistry of the lacustrine Wilkins Peak Member, Eocene Green River Formation, Wyoming, U.S.A. Ph.D. thesis, University of Wisconsin-Madison, 372 p

Pietras JT, Carroll AR, Rhodes MK (2003) Lake basin response to tectonic drainage diversion: Eocene Green River Formation, Wyoming. J Paleolimnol 30:115–125

Pipiringos GN (1955) Tertiary rocks in the central part of the Great Divide Basin, Sweetwater County, Wyoming. In: Anderman GG (ed) Green river basin, 10th annual field conference guidebook. Wyoming Geological Association, Casper, pp 100–104

Pitman JK (1996) Origin of primary and diagenetic carbonates in the lacustrine Green River Formation (Eocene), Colorado and Utah. US Geol Surv Bull 2157:17

Pitman JK, Norris RD, Jones LS, Corfield RM (1996) Effects of water-residence time on the isotopic evolution of an Eocene closed-basin lake complex. American Association of Petroleum Geologists and Society of Economic Paleontologists and Mineralogists annual meeting abstracts 5, p 113

Renaut RW, Gierlowski-Kordesch EH (2010) Lakes. In: James NP, Dalrymple RW (eds) Facies models 4, vol 6, Geotext. Geological Association of Canada, St. John's, pp 541–575

Rhodes MK (2002) Lacustrine stratigraphy and strontium isotope geochemistry of the Laney member, Green River Formation, southwestern Wyoming. Ph.D. thesis, University of Wisconsin-Madison, 367 p

Roehler HW (1991a) Correlation and depositional analysis of oil shale and associated rocks in the Eocene Green River Formation, Greater Green River Basin, southwest Wyoming. U.S. Geological Survey Miscellaneous investigations series Map I-2226

Roehler HW (1991b) Revised stratigraphic nomenclature for the Wasatch and Green River Formations of Eocene age, Wyoming, Utah, and Colorado, U.S. Geological Survey professional paper 1506-B. U.S. Government Printing Office, Washington, DC, p 38

Roehler HW (1992) Correlation, composition, areal distribution, and thickness of Eocene stratigraphic units, greater Green River basin, Wyoming, Utah, and Colorado, U.S. Geological Survey professional paper 1506-E. U.S. Dept. of the Interior, U.S. Geological Survey, Reston, p 49

Roehler HW (1993) Eocene climates, depositional environments, and geography, Greater Green River Basin, Wyoming, Utah, and Colorado, U.S. Geological Survey professional paper 1506-F. U.S. Government Printing Office, Washington, DC, p 74

Rosenbaum J, Sheppard SMF (1986) An isotopic study of siderites, dolomites, and ankerites at high temperatures. Geochim Cosmochim Acta 50:1147–1150

Scholz CA, Johnson TC, McGill JW (1993) Deltaic sedimentation in a rift valley lake; new seismic reflection data from Lake Malawi (Nyasa), East Africa. Geology 21:395–398

Schultz AR (1920) Oil possibilities in and around Baxter Basin, in the Rock Springs Uplift, Sweetwater County, Wyoming. US Geol Surv Bull 702:107

Sharma T, Clayton RN (1965) Measurement of O^{18}/O^{16} of total oxygen of carbonates. Geochim Cosmochim Acta 29:1347–1353

Smith ME, Carroll AR, Singer BS (2008) Synoptic reconstruction of a major ancient lake system: Eocene Green River Formation, Western United States. Geol Soc Am Bull 120:54–84

Smith ME, Chamberlain KR, Singer BS, Carroll AR (2010) Eocene clocks agree: coeval ^{40}Ar/^{39}Ar, U-Pb, and astronomical ages from the Green River Formation. Geology 38:527–530

Stanley KO, Surdam RC (1978) Sedimentation on the front of Eocene Gilbert-type deltas, Washakie Basin, Wyoming. J Sediment Petrol 48:557–573

Steidtmann JR (1969) Stratigraphy of the early Eocene Pass Peak Formation, central-western Wyoming. In:

Barlow JA (ed) Symposium on tertiary rocks of Wyoming, 21st annual field conference guidebook. Wyoming Geological Association, Casper, pp 55–63

Surdam RC, Stanley KO (1979) Lacustrine sedimentation during the culminating phase of Eocene Lake Gosiute, Wyoming (Green River Formation). Geol Soc Am Bull 90:93–110

Talbot MR (1990) A review of the palaeohydrological interpretation of carbon and oxygen isotopic ratios in primary lacustrine carbonates. Chem Geol 80:261–279

Talbot MR, Allen PA (1996) Lakes, 3. In: Reading HG (ed) Sedimentary environments; processes, facies and stratigraphy. Blackwell, Oxford, pp 83–124

Tissot BP, Vandenbroucke M (1983) Geochemistry and pyrolysis of oil shales. ACS Symp Ser 230:1–11

Walker JC (2008) Lacustrine stratigraphic and stable isotopic expression of overfilled and balanced-filled transitions within the Tipton Member of the Green River Formation. M.Sc. thesis, University of Wisconsin-Madison, 166 p

Westerhold T, Röhl U (2009) High resolution cyclostratigraphy of the early Eocene – new insights into the origin of the Cenozoic cooling trend. Clim Past 5:309–327

Witkind IJ, Grose LT (1972) Areal geologic map of the Rocky Mountain region and environs. In: Mallory WW (ed) Geologic Atlas of the Rocky Mountain Region. Rocky Mountain Association of Geologists, Denver, p 34

Wolfbauer CA, Surdam RC (1974) Origin of nonmarine dolomite in Eocene Lake Gosiute, Green River Basin, Wyoming. Geol Soc Am Bull 85:1733–1740

Zachos J, Pagani M, Sloan L, Thomas E, Billups K (2001) Trends, rhythms, and aberrations in global climate 65 Ma to present. Science 292:685–693

Zachos JC, Dickens GR, Zeebe RE (2008) An early Cenozoic perspective on greenhouse warming and carbon-cycle dynamics. Nature 451:279–283